Nonlinear relativistic single-electron Thomson scattering power spectrum for incoming laser of arbitrary intensity

R. F. Álvarez-Estrada, I. Pastor, J. Guasp, and F. Castejón

Citation: Phys. Plasmas **19**, 062302 (2012); doi: 10.1063/1.4725190
View online: http://dx.doi.org/10.1063/1.4725190
View Table of Contents: http://pop.aip.org/resource/1/PHPAEN/v19/i6
Published by the American Institute of Physics.

Nonlinear relativistic single-electron Thomson scattering power spectrum for incoming laser of arbitrary intensity

R. F. Álvarez-Estrada,[1,a)] I. Pastor,[2,b)] J. Guasp,[2] and F. Castejón[2,c)]
[1]*Departamento de Física Teórica I, Facultad de Ciencias Físicas, Universidad Complutense, 28040 Madrid, Spain*
[2]*Asociación Euratom/Ciemat para Fusión, Avenida Complutense 22, 28040 Madrid, Spain*

(Received 10 January 2012; accepted 12 April 2012; published online 8 June 2012)

The classical nonlinear incoherent Thomson scattering power spectrum from a single relativistic electron with incoming laser radiation of any intensity, investigated numerically by the present authors in a previous publication, displayed both an approximate quadratic behavior in frequency and a redshift of the power spectrum for high intensity incoming radiation. The present work is devoted to justify, in a more general setup, those numerical findings. Those justifications are reinforced by extending suitably analytical approaches, as developed by other authors. Moreover, our analytical treatment exhibits differences between the Doppler-like frequencies for linear and circular polarization of the incoming radiation. Those differences depend nonlinearly on the laser intensity and on the electron initial velocity and do not appear to have been displayed by previous authors. Those Doppler-like frequencies and their differences are validated by new Monte Carlo computations beyond our previuos ones and reported here. © *2012 American Institute of Physics*. [http://dx.doi.org/10.1063/1.4725190]

I. INTRODUCTION

The scattering of electromagnetic radiation by a fusion plasma is one of the most useful and powerful methods for diagnosis.[1] This applies, in particular, to classical incoherent Thomson scattering (TS) with adequately intense radiation sources, which is a standard diagnostic technique for electron temperature and density measurement in fusion devices. The basic understanding of this phenomenon is well documented, see for instance[2–8] and references therein. The usefulness of TS has continued to be manifest as the temperatures of the plasmas have increased through successive devices. The physics of classical incoherent TS still applies as typical electron temperatures increase from the several keV range up to tens of keV and more, provided that the relative importance of relativistic effects (mainly, the overall blue shift of the spectrum and the depolarization of scattered radiation) be taken into account accordingly. It is also clear that TS will continue to be a key diagnostic tool for the ITER tokamak, where electron temperatures in the range of 40 keV are expected when fully operational.[9] In the latter case, the relativistic effects will be increased with respect to former fusion devices, and some very weak nonlinear effects would develop arising from the high peak power of the lasers to be used (a few Joule in 200 ps pulse length). Therefore, relativistic (and, eventually, some weak nonlinear) effects in incoherent TS will be of key importance for interpreting the spectra in the future TS system of ITER. Moreover, it will also be mandatory to consider non-Maxwellian distribution functions in the current framework of incoherent TS, since their existence appears to show up in plasmas heated by energetic alpha particles. In fact, due to the structure of the distribution functions, incoherent TS could produce results different from other diagnostics like ECE (electron cyclotron emission), since they probe different regions of the velocity space.

While our interest here focuses exclusively on incoherent TS by relativistic electrons (which behave independently of each other), for completeness, one should remind recent investigations on other relativistic effects in TS of a different kind, namely, the collective scattering of laser radiation by electron-density fluctuations with relativistic phase velocities: see Ref. 10 for experimental observations and Ref. 11 for a fully relativistic theoretical analysis. As it is well known, incoherent and collective TS occur in certain regimes which are different from each other.[2]

We remind that the classical equations of motion for a relativistic electron subject to an incoming (non-necessarily monochromatic) electromagnetic plane wave have been solved exactly in an analytical (although implicit) way,[12] which provided the basis for subsequent approximate studies of incoherent TS,[13–18] by using the Liénard-Wiechert radiated fields.[19] Recently,[20] the present authors extended those researches. We shall remind in this section some basic ingredients for Ref. 20, which will also be essential here: the mathematical set-up for the incoming laser beam, the classical equations of motion for the electron subject to the former, a very short quantitative reminder of the exact solution for an incoming, non-necessarily monochromatic, plane wave radiation[12] (to be amplified in Appendix A, later), and the Liénard-Wiechert radiated fields[19] as the basis for an approximate application to incoherent TS. The results of Ref. 20 will also be summarized in this section. Further reference to Ref. 20 will be made when absolutely necessary in the main text and, when several detailed aspects and generalizations thereof be required, in Appendix A.

[a)]Electronic mail: rfa@fis.ucm.es.
[b)]Electronic mail: ignacio.pastor@ciemat.es.
[c)]Electronic mail: francisco.castejon@ciemat.es.

A. Incoming arbitrary non-monochromatic plane wave

Two time variables (t and t') were employed in Ref. 20 and will also be used here, with the same meanings. Their meanings, in the different contexts, will be reminded as we proceed here, and no confusion should arise.

The radiation (or Coulomb) gauge shall be employed. Let $\mathbf{A}_i$ be the transverse vector potential of the incoming electric and magnetic fields $\mathbf{E}_i$ and $\mathbf{B}_i$. $\mathbf{E}_i$, $\mathbf{B}_i$ and $\mathbf{A}_i$ depend on a three-dimensional position $\mathbf{y} = (y_1, y_2, y_3)$ and on time (t). One has in the radiation gauge

$$\nabla_{\mathbf{y}} \mathbf{A}_i = 0, \quad \mathbf{E}_i = -\frac{\partial \mathbf{A}_i}{\partial t}, \quad \mathbf{B}_i = \nabla_{\mathbf{y}} \times \mathbf{A}_i \,. \tag{1}$$

The input beam field, corresponding to an arbitrary non-monochromatic plane wave and fulfilling the charge-free Maxwell equations in vacuum, propagates along the y_3 axis, from $-\infty$ towards $+\infty$. The divergenceless $\mathbf{A}_i(\mathbf{y};t) = \mathbf{A}_i(\xi)$, where $\xi \equiv t - y_3/c$ (c being the velocity of light in vacuum), lies in the (y_1, y_2)-plane

$$\begin{aligned} &\mathbf{A}_i = (\bar{A}_i, 0), \quad \bar{A}_i = \bar{A}_i(\xi) = (A_{i,1}, A_{i,2}), \\ &\mathbf{E}_i = -\mathbf{A}_i', \quad \mathbf{B}_i = c^{-1}\mathbf{k} \times \mathbf{E}_i \end{aligned} \tag{2}$$

with $\mathbf{A}_i' \equiv d\mathbf{A}_i/d\xi$, and $\mathbf{k} = (0,0,1)$ being the unit vector along the y_3 axis. We emphasize that variables with overbars will always denote two-dimensional vectors in the (y_1, y_2)-plane: such variables will also be employed in Appendix A. In the simplest case, the incoming laser field is represented by a purely monochromatic plane wave. Then, for a linearly polarized plane wave,

$$\mathbf{E}_i = \mathbf{j} E_0 \cos \omega_0 \left[t - \frac{y_3}{c} \right] . \tag{3}$$

Another simple application is a circularly polarized plane wave

$$\mathbf{E}_i = E_0 \left(\mathbf{i} \cos \omega_0 \left[t - \frac{y_3}{c} \right] + \mathbf{j} \sin \omega_0 \left[t - \frac{y_3}{c} \right] \right) . \tag{4}$$

In both Eqs. (3) and (4), E_0 is a real amplitude and ω_0 (real and > 0) is the frequency.

The intensity of the incoming laser field is characterized by the dimensionless parameter $\alpha = (|e|E_0\lambda)/(mc^2)$. $e(<0)$ and m are the electron charge and mass, respectively, and $\lambda = (2\pi c)/\omega_0$ is the incoming wavelength. As an illustration, the Q-switched (FWHM $\simeq$ 20 ns and $E \simeq$ 10 J) and focused (2 mm diameter) ruby laser used for Thomson scattering in the TJ-II Stellarator (Laboratorio Nacional de Fusión, CIEMAT) has $\alpha \simeq 5.0 \times 10^{-4}$.

B. Classical equations of motion for the electron

We shall make use of the MKS system of units (see, for instance, Ref. 19) throughout the paper. We shall consider, in the infinite three-dimensional space, a classical relativistic electron with position vector $\mathbf{x}(= \mathbf{x}(t))$ and momentum $\mathbf{p} = \mathbf{p}(t)$ at time t, in vacuum. The electron interacts with the classical electromagnetic field in vacuum. The electromagnetic field is the sum of an incoming (subscript i) field and of the dynamical field radiated by the electron itself (after its initial free motion is perturbed by the input beam field). The incoming electromagnetic field is described by $\mathbf{E}_i$ and $\mathbf{B}_i$ which, by assumption, correspond to a (in general, non-monochromatic) plane-wave radiation. Let $\mathbf{E}$ and $\mathbf{B}$ be the total electric and magnetic fields, respectively. All of them also depend on $\mathbf{y}$ and on t.

In order to solve the dynamical problem, an approximation method is used, based on the assumption that $\mathbf{E}$ and $\mathbf{B}$ can be replaced, respectively, by $\mathbf{E}_i$ and $\mathbf{B}_i$. Then, the equations of motion of the relativistic electron subject to the Lorentz force of the incoming electric and magnetic fields $\mathbf{E}_i = \mathbf{E}_i(\mathbf{y} = \mathbf{x}(t), t)$ and $\mathbf{B}_i = \mathbf{B}_i(\mathbf{y} = \mathbf{x}(t), t)$ read[12] ($\gamma(t) = [1 - c^{-2}(d\mathbf{x}/dt)^2]^{-1/2}$)

$$\mathbf{p} = m\gamma(t)\frac{d\mathbf{x}}{dt}, \quad \frac{d\mathbf{p}}{dt} = e\mathbf{E}_i + e\frac{d\mathbf{x}}{dt} \times \mathbf{B}_i. \tag{5}$$

Notice that $d\mathbf{x}/dt = c^2\mathbf{p}/[m^2c^4 + c^2\mathbf{p}^2]^{1/2}$. With the above understanding for $\mathbf{E}_i(\mathbf{y} = \mathbf{x}(t), t)$ and $\mathbf{B}_i(\mathbf{y} = \mathbf{x}(t), t)$, the dynamical problem boils down to solve the non-linear Eq. (5) for the electron position $\mathbf{x}(t)$ and momentum $\mathbf{p}(t)$ at time t. Let $\boldsymbol{\beta}_0$ be some suitable normalized initial velocity of the electron (that is, c^{-1} times certain suitable initial velocity), before receiving and being affected by the incoming monochromatic plane wave created by the laser. We write $\boldsymbol{\beta}_0 = (\beta_{01}, \beta_{02}, \beta_{03}) = \beta_0(\sin\theta\cos\varphi, \sin\theta\sin\varphi, \cos\theta)$. We shall consider a general case in which $\boldsymbol{\beta}_0$ is not orthogonal to $\mathbf{A}_i$: $\boldsymbol{\beta}_0.\mathbf{A}_i \neq 0$. Suitable initial position of the electron and $\boldsymbol{\beta}_0$ will provide the initial conditions to solve Eq. (5) see Appendix A. It is important noting that the differential Eq. (5) can be exactly solved for the case of an incoming (non-necessarily monochromatic) plane wave, the solution being given in an analytical (although implicit) way.[12–17] See also Ref. 18 for a recent account of the exact solutions, which the authors of that work also deem important as a basis for the computation of Thomson scattering spectra.

The detailed exact solution is outlined in Appendix A, and it is used in Sec. II where the Liénard-Wiechert fields are transformed from the time domain to the frequency domain.

The radiated Liénard-Wiechert fields do not (in the approximation scheme used here) perturb the electric and magnetic fields responsible for the electron motion, which are always the laser fields only. In particular, this implies that the effect of radiation reaction and the possibility of run-away solutions (a controversial feature associated to the Abraham-Lorentz equation)[12,19,21] are excluded from the outset. It has been argued that radiation reaction effects could induce a significant alteration of the electron motion over a sufficiently long time interval: see Ref. 13 and references therein. On the other hand, radiation reaction effects are quantitatively small in a wide variety of situations,[12,19,21] and one could also argue that the latter may include those having interest here. Run-away solutions have been shown to be absent in a consistent treatment: see Ref. 22 (provided a suitable cut-off procedure be imposed) and references therein (for other treatments).

C. Liénard-Wiechert retarded radiation fields

Let $\mathbf{E}(\mathbf{y},t)_{rr}$ and $\mathbf{B}(\mathbf{y},t)_{rr}$ be the Liénard-Wiechert retarded radiation fields (subscript *rr*) at the position $\mathbf{y}$ at ("detection") time t (Refs. 19 and 20) for any incoming (in general, non-monochromatic) radiation. They read

$$\mathbf{E}(\mathbf{y},t)_{rr}=\frac{e\left[\mathbf{r}\times\left(\left(\mathbf{r}-\frac{r}{c}\frac{d\mathbf{x}(t')}{dt'}\right)\times\frac{d^2\mathbf{x}(t')}{dt'^2}\right)\right]}{4\pi\epsilon_0 c^2[r-c^{-1}\mathbf{r}(d\mathbf{x}(t')/dt')]^3}\,, \tag{6}$$

$$\mathbf{B}(\mathbf{y},t)_{rr}=\frac{\mathbf{r}}{cr}\times\mathbf{E}(\mathbf{y},t)_{rr}, \tag{7}$$

ϵ_0 is the dielectric permittivity of vacuum. Both $\mathbf{E}(\mathbf{y},t)_{rr}$ and $\mathbf{B}(\mathbf{y},t)_{rr}$ depend nonlinearly on $\mathbf{x}(t')$, the solution of Eq. (5) at the "radiation" time t' and, hence, on the input beam fields. For given detector position $\mathbf{y}$ and "detection" time t, the time t' is obtained from: $c(t-t')=\mid\mathbf{y}-\mathbf{x}(t')\mid$. In many TS systems, it is a good approximation to consider that the observation point (the point where the detector lies) is located far away from the radiating electron. Therefore, we assume that the electron is about or not far from the origin of coordinates initially and does not separate too much from it in the course of its interaction with the laser. Then, Eqs. (6) and (7) for $\mathbf{E}(\mathbf{y},t)_{rr}\simeq\mathbf{E}(\mathbf{y},t)_{rr,\infty}$ and $\mathbf{B}(\mathbf{y},t)_{rr}\simeq\mathbf{B}(\mathbf{y},t)_{rr,\infty}$ become for the asymptotic fields

$$\mathbf{E}(\mathbf{y},t)_{rr,\infty}=\frac{e\mathbf{n}\times[(\mathbf{n}-\boldsymbol{\beta})\times(d^2\mathbf{x}/dt'^2)]}{4\pi\epsilon_0 c^2 R[1-\mathbf{n}.\boldsymbol{\beta}]^3}, \tag{8}$$

$$\mathbf{B}(\mathbf{y},t)_{rr,\infty}=\frac{\mathbf{n}}{c}\times\mathbf{E}(\mathbf{y},t)_{rr,\infty} \tag{9}$$

with $R=\mid\mathbf{y}\mid$, $\mathbf{n}=R^{-1}\mathbf{y}$ and $\boldsymbol{\beta}\equiv c^{-1}(d\mathbf{x}/dt')=(\beta_1,\beta_2,\beta_3)$. $\mathbf{n}$ (the scattering unit vector) indicates the direction at which a detector is located at $\mathbf{y}$. Both $\boldsymbol{\beta}$ and the acceleration of the relativistic electron $d^2\mathbf{x}/dt'^2$ in Eqs. (8) and (9) are taken at a time t' such that $t'-c^{-1}\mathbf{n}.\mathbf{x}(t')=t-c^{-1}R$ and $R\gg\mid\mathbf{x}(t')\mid$. The asymptotic Poynting vector is $\mu_0^{-1}\mathbf{E}(\mathbf{y},t)_{rr,\infty}\times\mathbf{B}(\mathbf{y},t)_{rr,\infty}$, μ_0 being the magnetic permeability of vacuum. The flow of radiated energy per unit time and unit area, determined by the Poynting vector at $\mathbf{y}$ and along $\mathbf{n}$, is[19] $\epsilon_0 c\mathbf{E}(\mathbf{y},t)^2_{rr,\infty}$, $\mathbf{E}(\mathbf{y},t)_{rr,\infty}$ being given in Eq. (8). We consider that a tiny spectrally flat (ideal) detector, placed at $\mathbf{y}$ and perpendicular to $\mathbf{n}$, receives and measures the time average of $\epsilon_0 c\mathbf{E}(\mathbf{y},t)^2_{rr,\infty}$ (referred to in Ref. 20 as mean power or scattered power spectrum of the radiated field in a, perhaps, loosely way). It is understood that such an expression for the time average includes the sum over the two possible orthogonal polarizations of the radiated field, but they can be accounted for separately if needed.

Typically, $\mathbf{n}(=n_1,n_2,n_3)$, with $(n_1^2+n_2^2+n_3^2=1)$, is chosen to be orthogonal to $\mathbf{j}$: $\mathbf{n}=\mathbf{n}_0=\sin\theta_0\mathbf{i}+\cos\theta_0\mathbf{k}$ (hence, the scattering vector lies in the (y_1,y_3) plane). This scattering geometry encompasses both the one used for TS at the TJ-II Stellarator at CIEMAT ($\theta_0=\pi/2$), and the backscattering geometry proposed for the ITER tokamak ($\theta_0=\pi$).

D. The previous Monte Carlo approach: Results

In our previous work,[20] the resulting solution for $\mathbf{x}(t)$ obtained from the numerical integration of Eq. (5) (also shown there to fully agree with the analytical solution[12]) was used (with t replaced by t') to evaluate the dynamical electromagnetic field radiated by the particle, by plugging the former directly into the standard $\mathbf{E}_{rr,\infty}$ and $\mathbf{B}_{rr,\infty}$.[19] That was the approach of the Monte Carlo technique developed in Ref. 20. From the trajectory obtained numerically, the Liénard-Wiechert retarded fields computed at detector place and the use of FFT (fast Fourier transform) techniques, the TS spectrum from a sample of electrons with predefined distribution function was computed. Thus, the Monte Carlo technique was shown to provide results in excellent agreement with analytical results, and to be able to extend the computation of TS spectra to regimes where these are difficult to get, for example, when the laser intensity is so high that nonlinear effects must be taken into account. The computation of TS spectra for (essentially) monoenergetic and isotropic electron distribution functions (EDFs) showed a neat ω^2 dependence for energies of up to several hundreds keV and for very low values of the laser parameter α. As it was argued that these monoenergetic distributions form the basis for more general EDFs, an attempt was made in the previous paper to justify that ω^2 dependence, using a mixed approach involving both analytical and Monte Carlo computations. Another result from the Monte Carlo computations, which will also be addressed in this paper, was the observation of an overall redshift of scattered spectrum when the electrons were acted by a laser with α of the order of one.

E. Purpose and plan of the present work

The present paper originates on further attempts to justify the approximate ω^2 dependence and to extend other results presented in our previous publication,[20] in a more general setup. In this connection, the monograph of Avetissian[17] will be of unvaluable help. Results given in Ref. 17 will be generalised here. In fact, explicit formulas for the overall redshift of spectra as a function of the laser parameter will be given here, showing that the dependence is different for linear and circular polarization, which, in hindsight, explains some numerical findings reported in Ref. 20.

The present paper is organized as follows. Section II is devoted to the spectral representation of the Liénard-Wiechert radiation fields and their connection with the TS power spectrum. In that section, explicit formulas are given for the amplitudes of the different harmonics, which contribute to the scattered spectrum (since the treatment includes the case of ultraintense laser radiation). Sections III and IV apply the formalism of Sec. II to linearly and circularly polarized monochromatic radiation, respectively: the different behaviors are highlighted and compared with new Monte Carlo computations of TS spectra for selected energy distribution functions, and certain analytical results obtained in Sec. II are cast into forms suitable for fast and efficient computation of TS spectra for a wide range of values of the laser parameter. Section V discusses, in a compact way, the consequences of the previous sections regarding power spectra, quadratic behavior in frequency and redshifts. Section VI contains the conclusions and some discussion/prospects for

future work. Appendix A summarizes the solutions of the classical equations of motion for the electron subject to an incoming plane wave radiation (either linearly or circularly polarized) and includes new aspects, in particular, the issue of gauge invariance of those solutions. Appendix B collects certain useful coefficients that are defined and employed in Secs. II–IV. Appendix C discusses in outline the generalized Bessel Functions appearing in the spectral representation of Liénard-Wiechert retarded radiation fields (for linear polarization).

II. SPECTRAL ASYMPTOTIC LIÉNARD-WIECHERT RETARDED RADIATION FIELDS AND POWER

A. Integral representations

We shall introduce the spectral (or frequency Fourier transforms of the) asymptotic Liénard-Wiechert retarded radiation fields given in Eqs. (8) and (9)

$$\tilde{\mathbf{B}}(\mathbf{y},\omega)=\int_{-\infty}^{+\infty}\frac{dt}{(2\pi)^{1/2}}\exp(i\omega t)\mathbf{B}(\mathbf{y},t)_{rr,\infty} \tag{10}$$

and so on for $\tilde{\mathbf{E}}(\mathbf{y},\omega)(\simeq -c\mathbf{n}\times\tilde{\mathbf{B}}(\mathbf{y},\omega))$. Below, we shall employ some standard transformations,[16,17,21,23] allowing to reduce the above spectral asymptotic fields to more amenable representations for the case of a general non-monochromatic incoming plane wave, thereby extending directly the integral representations treated in Ref. 17, which are restricted to incoming purely monochromatic plane waves. It will suffice to concentrate on $\tilde{\mathbf{B}}(\mathbf{y},\omega)$. We shall carry out the following successive transformations.[21,23] (i) We perform a change of integration variable from t ("detection" time) to t' ("radiation" time), with $t'-c^{-1}\mathbf{n}.\mathbf{x}(t')=t-c^{-1}R$. (ii) After (i), we carry out an integration by parts, in t' and discard (as argued in Refs. 21 and 23) the integrated or ("surface") contributions from $t'\to+\infty$ and $t'\to-\infty$. We get

$$\tilde{\mathbf{B}}(\mathbf{y},\omega)=\frac{i\omega e\exp(i\omega R/c)}{4\pi\epsilon_0 c^2 R}\int_{-\infty}^{+\infty}\frac{dt'}{(2\pi)^{1/2}}\left[\frac{\mathbf{n}}{c}\times\frac{d\mathbf{x}}{dt'}\right]\times\exp[i\omega(t'-c^{-1}\mathbf{n}\mathbf{x}(t'))]. \tag{11}$$

For the last transformations, we shall follow.[17] Thus (iii) we eliminate $d\mathbf{x}/dt'$ in terms of $\mathbf{p}$ in $(\mathbf{n}/c)\times(d\mathbf{x}/dt')$ in Eq. (11), by using $d\mathbf{x}/dt'=c^2\mathbf{p}/[c(\gamma_1+p_3(\xi))]$. γ_1 is a constant of motion. Let $\xi=t'-(x_3/c)$ be the "wave" coordinate. See Appendix A for it and for γ_1, and recall Eqs. (A6) and (A7). Finally, (iv) we perform a second change of variables, now from t' to ξ. In so doing, we employ $dt'/[c(\gamma_1+p_3(\xi))]=d\xi/(c\gamma_1)$. We thus arrive at

$$\tilde{\mathbf{B}}(\mathbf{y},\omega)=\frac{i\omega e\exp(i\omega R/c)}{4\pi\epsilon_0 c^2\gamma_1 R}[\mathbf{n}\times\tilde{\mathbf{p}}(\mathbf{y},\omega)], \tag{12}$$

$$\tilde{\mathbf{p}}(\mathbf{y},\omega)=\int_{-\infty}^{+\infty}\frac{d\xi}{(2\pi)^{1/2}}\mathbf{p}(\xi)\exp[i\omega\Lambda(\xi)], \tag{13}$$

$$\Lambda(\xi)=t'-c^{-1}\mathbf{n}\mathbf{x}(t')=\xi+\frac{x_3(t')-\mathbf{n}\mathbf{x}(t')}{c}, \tag{14}$$

$$\Lambda(\xi)=\xi+\frac{(1-\cos\theta_0)x_3(\xi)-\sin\theta_0 x_1(\xi)}{c}. \tag{15}$$

Notice that $\tilde{\mathbf{B}}(\mathbf{y},-\omega)=(\tilde{\mathbf{B}}(\mathbf{y},\omega))^*$ and $\tilde{\mathbf{p}}(\mathbf{y},-\omega)=(\tilde{\mathbf{p}}(\mathbf{y},\omega))^*$. Recall that t' can be expressed formally in terms of ξ, by employing the solutions of the equations of motion (5). Fortunately, no such analytical work is needed in practice regarding $\tilde{\mathbf{p}}(\mathbf{y},\omega)$, since x_1, x_2, and x_3 are given directly in terms of ξ through Eqs. (A1) and (A2). The components p_1, p_2, and p_3 of $\mathbf{p}(\xi)$ are also given directly in terms of ξ through Eqs. (A4) and (A5) and Eq. (A9) given in Appendix A. Equation (15), to be employed later, is the restriction of Eq. (14) to the case $\mathbf{n}=\mathbf{n}_0$. An analogous representation follows for $\tilde{\mathbf{E}}(\mathbf{y},\omega)$, by using $\tilde{\mathbf{E}}(\mathbf{y},\omega)\simeq -c\mathbf{n}\times\tilde{\mathbf{B}}(\mathbf{y},\omega)$. Equations (A1)–(A5) giving $\mathbf{x}(\xi)$ and $\mathbf{p}(\xi)$ depend on $\bar{A}_i$, which is not uniquely defined, so that the question whether the former are uniquely determined arises. The analysis in Appendix A (Eq. (A8)) shows that $\mathbf{x}(\xi)$ and $\mathbf{p}(\xi)$ are independent on the choice of $\bar{A}_i$ and, hence, the same conclusion holds for $\tilde{\mathbf{B}}(\mathbf{y},\omega)$ and $\tilde{\mathbf{E}}(\mathbf{y},\omega)$.

The following additional discussion is adequate. Once one has obtained the exact solution of Eq. (5) for a (in general, non-monochromatic) plane-wave radiation, as outlined in Appendix A, the computation of the asymptotic Liénard-Wiechert retarded radiation fields $\mathbf{E}(\mathbf{y},t)_{rr,\infty}$ and $\mathbf{B}(\mathbf{y},t)_{rr,\infty}$ in Eqs. (8) and (9) requires to solve $t'-c^{-1}\mathbf{n}.\mathbf{x}(t')=t-c^{-1}R$ with $R\gg|\mathbf{x}(t')|$ numerically, as was done in Ref. 20. On the other hand, Eqs. (12) and (13) and the corresponding one for $\tilde{\mathbf{E}}(\mathbf{y},\omega)$ enable to compute the spectral fields $\tilde{\mathbf{B}}(\mathbf{y},\omega)$ and $\tilde{\mathbf{E}}(\mathbf{y},\omega)$ just by evaluating those integrals over ξ (numerically or through some approximate analytical method), without needing to solve for the implicit equation $t'-c^{-1}\mathbf{n}.\mathbf{x}(t')=t-c^{-1}R$. We emphasize the fact that $\Lambda(\xi)$ in Eq. (15) contains only powers of $\bar{A}_i$ not higher than two. This simplification follows exactly from the above changes of integration variables and is very far-reaching. That simplification holds in spite of the fact that the exact solution of Eq. (5) given through Eqs. (A1), (A2) and (A4), (A5) is only an implicit one and, hence, simple only in an apparent sense. In fact, it is intrinsically highly nonlinear, as discussed in Appendix A.

Recall that the total radiated energy (U) in the unit solid angle (Ω) around $\mathbf{n}$ for large $R=|\mathbf{y}|$, at all "detection" times t, is $dU/d\Omega=R^2\epsilon_0 c\int_{-\infty}^{+\infty}dt\mathbf{E}(\mathbf{y},t)^2_{rr,\infty}=2R^2\epsilon_0 c^3\int_0^{+\infty}d\omega|\tilde{\mathbf{B}}(\mathbf{y},\omega)|^2$. Then, the spectral density of the total radiated energy, per unit solid angle and unit frequency interval (for positive frequencies), is

$$\frac{d^2U}{d\Omega d\omega}=2R^2\epsilon_0 c^3|\tilde{\mathbf{B}}(\mathbf{y},\omega)|^2=F_0|\mathbf{n}\times\tilde{\mathbf{p}}(\mathbf{y},\omega)|^2, \tag{16}$$

$$F_0=\frac{e^2\omega^2}{8\pi^2\epsilon_0 c\gamma_1^2}. \tag{17}$$

Physically, the "detection" time t does not vary in $(-\infty,+\infty)$, but in a very large interval, and the same applies to t' and ξ. The above spectral energy density in Eq. (16), which refers to an arbitrarily (mathematically, an

infinitely) large time interval, is very large (mathematically, diverges) for an incoming monochromatic plane wave. Such a physical divergence, which is natural, is proportional to the very (infinitely) large time duration or temporal extension of that plane wave, as we shall see later in Subsections III C and IV C (where the divergence will be cured). The numerical computations of the radiated energy in Ref. 20 were based upon an incoming monochromatic plane wave, which was not infinitely extended: rather, we considered a large number of cycles of the latter, within a very large interval.

B. Incoming monochromatic radiation

We shall consider an incoming strictly monochromatic plane wave with frequency ω_0. We shall let $\mathbf{n} = \mathbf{n}_0$ and make use of the index δ and of the coefficient c_δ. They enable to treat either linear ($\delta = L$) or circular ($\delta = C$) polarization in a compact way. We choose $c_{\delta=L} = 0$, while $c_{\delta=C} = 1$. We employ Eq. (A23) in this work and Eq. (B13) in Ref. 20 for a linearly (L) polarized wave and of Eq. (A25) in this work and Eq. (B18) in Ref. 20 for a circularly (C) polarized one. Then, for both linearly and circularly polarized waves, $\Lambda(\xi) = \Lambda(\xi)_\delta$ in Eq. (15) is given by

$$\Lambda(\xi)_\delta = \frac{1}{\omega_0}(g_{0,\delta} + g_{1,\delta}\omega_0\xi + g_{2,\delta}\sin(\omega_0\xi - \varphi_\delta) - g_{3,\delta}\sin 2\omega_0\xi), \tag{18}$$

$$g_{0,\delta} = -\sin\theta_0\left[\frac{\omega_0 x_{0,1}}{c} + c_\delta\frac{eE_0}{\gamma_1\omega_0}\right] + (1-\cos\theta_0) \times \left[\frac{\omega_0 x_{3,0}}{c} + \frac{eE_0(f_1 c_\delta + f_2(1-c_\delta))}{\gamma_1^2\omega_0}\right], \tag{19}$$

$$g_{1,\delta} = 1 - \frac{f_1\sin\theta_0}{\gamma_1} + (1-\cos\theta_0) \times \left[\frac{s}{c} + \frac{eE_0}{\gamma_1^2\omega_0}\left(f_2 c_\delta + \frac{eE_0}{\omega_0(2-c_\delta)^2}\right)\right], \tag{20}$$

$$g_{2,\delta}\cos\varphi_\delta = -c_\delta(1-\cos\theta_0)\frac{eE_0(f_2 + (eE_0/\omega_0))}{\gamma_1^2\omega_0}, \tag{21}$$

$$g_{2,\delta}\sin\varphi_\delta = (1-c_\delta)(1-\cos\theta_0)\frac{eE_0 f_2}{\gamma_1^2\omega_0} + c_\delta \times \left[-\sin\theta_0\frac{eE_0}{\gamma_1\omega_0} + (1-\cos\theta_0)\frac{eE_0 f_1}{\gamma_1^2\omega_0}\right], \tag{22}$$

$$g_{3,\delta} = (1-c_\delta)\frac{(1-\cos\theta_0)(eE_0)^2}{8\gamma_1^2\omega_0^2}. \tag{23}$$

The parameters s, f_1 and f_2 are defined in Appendix A. With the definitions given above, the coefficients $g_{n,\delta}$, $n = 0,1,2,3$, and $\delta = C$, L are dimensionless and can be conveniently recast in terms of the laser parameter, the scattering angle, and the normalized initial position and momentum. The resulting formulas for $g_{n,\delta}$ are collected in Appendix B. We emphasize that the treatment given here includes the case in which the initial electron velocity is not necessarily parallel to the propagation of the incoming plane wave radiation, that is, $\boldsymbol{\beta}_0.\mathbf{A}_i$ may be $= 0$ or $\neq 0$.

In order to compute $\tilde{\mathbf{p}}(\mathbf{y},\omega)$, let us introduce the following scalar functions ($n = 0, \pm1, \pm2$):

$$b_{n,\delta} = \int_{-\infty}^{+\infty}\frac{d\xi}{(2\pi)^{1/2}}\exp[i\omega\Lambda(\xi)_\delta + in\omega_0\xi] = b_{n,\delta}(\omega). \tag{24}$$

Notice that $b_{n,\delta}(-\omega) = [b_{-n,\delta}(\omega)]^*$, where $*$ denotes the complex conjugate. Both $\tilde{\mathbf{p}}(\mathbf{y},\omega) = \tilde{\mathbf{p}}(\mathbf{y},\omega)_{\delta=L} = (\tilde{p}_{L,1}, \tilde{p}_{L,2}, \tilde{p}_{L,3})$ for linearly polarized plane waves and $\tilde{\mathbf{p}}(\mathbf{y},\omega) = \tilde{\mathbf{p}}(\mathbf{y},\omega)_{\delta=C} = (\tilde{p}_{C,1}, \tilde{p}_{C,2}, \tilde{p}_{C,3})$ for circularly polarized ones (recall Eq. (13)) can be expressed in terms of the scalar $b_{n,\delta}$'s. The specific equations will be given in Eqs. (28) and (41).

The computation of the scalars $b_{n,\delta}$ will be subsequently done by using series of the so-called generalized Bessel functions $J_l(x,y)$ (discussed below) for the case of linear polarization ($l = 0, \pm1, \pm2, \pm3, ...$) and of ordinary Bessel functions for the case of circular polarization ($J_l(z)$, $l = 0, \pm1, \pm2, \pm3, ...$, $J_{-l}(z) = (-1)^l J_l(z)$).[24]

Gathering all the results obtained up to now, the Thomson scattering spectral energy density (per unit solid angle and unit frequency interval) in Eq. (16) becomes for incoming monochromatic radiation and $\mathbf{n} = \mathbf{n}_0$:

$$\frac{d^2U}{d\Omega d\omega} = \left[\frac{d^2U}{d\Omega d\omega}\right]_\delta = F_0[|\cos\theta_0\tilde{p}_{\delta,1} - \sin\theta_0\tilde{p}_{\delta,3}|^2 + |\tilde{p}_{\delta,2}|^2]. \tag{25}$$

$\tilde{\mathbf{p}}(\mathbf{y},\omega)_\delta = (\tilde{p}_{\delta,1}, \tilde{p}_{\delta,2}, \tilde{p}_{\delta,3})$ are given through Eqs. (28) and (24) for linearly polarized radiation and through Eqs. (41) and (24) for circularly polarized radiation. In Secs. III and IV, the expression for the power spectrum will be critically analyzed, and its potential as a numerical tool for TS spectrum computation when a sample of electrons is considered, will be discussed.

III. MONOCHROMATIC LINEARLY POLARIZED RADIATION

A. The scalar function $b_{n,L}$ and the $\tilde{p}_{L,j}$'s

Let us begin with the case of incoming linearly polarized radiation ($\delta = L$), for which $\cos\varphi_{\delta=L} = 0$. Use will be made of the generalized Bessel functions $J_l(x,y)$. For an account of the latter, see Ref. 25 and references therein. In agreement with Ref. 25, the $J_l(x,y)$'s will be defined through the generating expression

$$\exp[i(x\sin(\theta-\varphi) - y\sin 2(\theta-\varphi))] = \sum_{l=-\infty}^{+\infty} J_l(x,y) \times \exp[il(\theta-\varphi)]. \tag{26}$$

See Appendix C for two representations of the generalized Bessel function $J_l(x,y)$ and other properties: in particular, $J_l(x,y)$ is shown to be real. We consider Eq. (26) for $\varphi = -\pi/2$. By plugging its complex conjugate into $b_{n,L}(\mathbf{y},\omega)$ (Eq. (24) for $\delta = L$), one finds ($\omega_r = \omega/\omega_0$)

$$b_{n,L} = \frac{(2\pi)^{1/2}}{\omega_0}\exp[i\omega_r g_{0,L}] \sum_{l'=-\infty}^{+\infty} J_{l'+n}(\omega_r g_{2,L}, \omega_r g_{3,L}) \times \exp\left[-i(l'+n)\frac{\pi}{2}\right]\delta(\omega_r g_{1,L} - l'), \quad (27)$$

δ denoting now the Dirac delta function (not to be confused with the subscript δ). Equation (27), as it stands, holds for $\varphi_{\delta=L} = \pi/2$ (with $g_{2,L} > 0$ and $f_2 > 0$) and for $\varphi_{\delta=L} = 3\pi/2$ (with $g_{2,L} < 0$ and $f_2 < 0$). Equivalently, for $\varphi_{\delta=L} = 3\pi/2$ (with $g_{2,L} > 0$ and $f_2 < 0$), Eq. (27) holds with $\exp[-i(l'+n)\frac{\pi}{2}]$ replaced by $\exp[i(l'+n)\frac{\pi}{2}]$. One has

$$\tilde{p}_{L,j} = mc\sum_{n=-2}^{+2} q_{L,jn} b_{n,L}, \quad j = 1,2,3. \quad (28)$$

The coefficients $q_{L,jn}$ are dimensionless. Their detailed expressions in terms of the laser parameter, etc. are given in Appendix B. The algebraic computations yielding Eq. (28) make use of Eqs. (3), (A4), and (A5) (or, alternatively, of Eqs. (B.16) and (B.17) for $\delta = L$ from Ref. 20, not reproduced here, for brevity).

B. Doppler-like formulas: Laser-parameter dependence

It is very important to realize that the only non-vanishing contributions to $b_{n,L}(\mathbf{y}, \omega)$ (by virtue of the δ's in Eq. (27)) are obtained for scattered frequencies $\omega = \omega_{L,l'}$ that fulfill the generalized Doppler-like formula

$$\omega_{L,l'} = \frac{l'\omega_0}{g_{1,L}} \quad (29)$$

for the given $g_{1,L}$ (see Eq. (20)) and for all the integers l' $(= 0, \pm1, \pm2, \pm3, ...)$. If ω varies in a finite interval, then only a discrete set of values for l' contribute. Moreover, the behaviors of the $J_{l'+n}(\omega_r g_{2,L}, \omega_r g_{3,L})$'s also play a role in the values of the power, although we shall not address that specifically in this work. For low values of the dimensionless laser parameter α (discussed in Subsection I A), only the harmonic with $l' = 1$ will contribute to the spectrum, but as the laser parameter grows, it is expected (and backed up by the numerical Monte Carlo computations in Ref. 20) that power will be found at higher harmonics ($l' > 1$). Equation (29) for linearly polarized laser radiation does depend on the laser parameter. Then, Eq. (29) generalizes the Doppler formula (independent on both the laser parameter and on the polarization properties of the incoming radiation), which was obtained from quantum mechanical energy-momentum conservation in Ref. 20 under certain approximations.

We shall write Eq. (29) more explicitly as follows:

$$\omega_{L,l'} = \frac{l'\omega_0(1-\beta_{03})}{1 - \mathbf{n}_0.\boldsymbol{\beta}_0 + (1-\cos\theta_0)\left[\frac{1-\boldsymbol{\beta}_0^2}{1-\beta_{03}}\right]\left[\frac{\alpha}{4\pi}\right]^2}. \quad (30)$$

The generalized Doppler formula (30), due to the α^2 term, predicts a redshift of the scattered frequency for very intense laser radiation. Equation (30) can be conveniently recast as $(\gamma_0 = [1-\boldsymbol{\beta}_0^2]^{-1/2})$

$$\omega_{L,l'} = \frac{l'\omega_0(1-\beta_{03})}{1 - \mathbf{n}_0.\boldsymbol{\beta}_0 + \left[\frac{\alpha}{4\pi\gamma_0}\right]^2(1-\cos\theta_0)/(1-\beta_{03})}. \quad (31)$$

Overall redshifts in scattered spectra for ultraintense lasers (which should not be qualified as kinematical, seemingly, but, rather, as dynamical ones) were reported in our previous publication,[20] but now a quantitative comparison with the Monte Carlo computations carried out there can be made. A systematic check of the Doppler formula (31) has been made, for monoenergetic and isotropic electron distribution functions of 25 keV and 100 keV, and for several values of the α parameter and the scattering angle θ_0, versus new Monte Carlo computations, which extend the previous ones.[20] For displaying the new Monte Carlo computations, we continue to make use of certain suitably normalized TS power spectrum distribution function $S^2(\omega)$ (power spectra, for short) previously employed.[20] The comparison between the bounds predicted by the above Doppler formula (31) and the new Monte Carlo computations for $S^2(\omega)$ has always been excellent. See Figs. 1–3.

It is important to compare Eq. (30) (with a quadratic dependence on the laser parameter) with a generalized Doppler formula obtained by Avetissian for both linearly and circularly polarized incident radiation. Avetissian's formula results from the vanishing of the arguments of the δ functions in Eq. (1.58) in Ref. 17. After some amount of algebraic computation, one can show that the generalized Doppler formula in Ref. 17 coincides with our Eq. (30) for linearly polarized incident radiation.

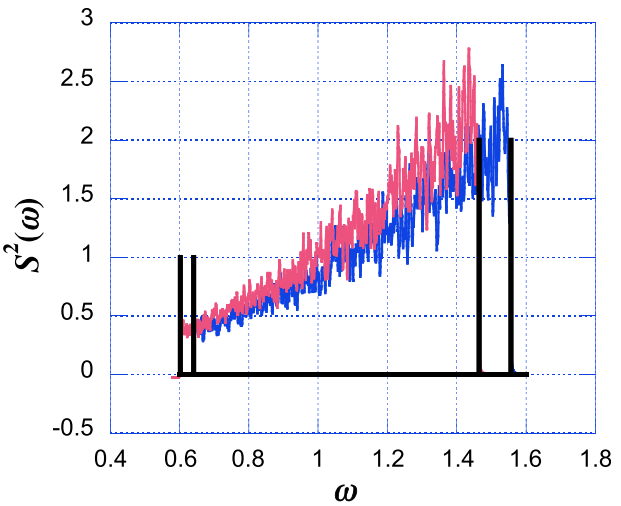

FIG. 1. Thomson scattering spectra from a monoenergetic, isotropic electron distribution function at 25 keV. $\theta_0 = \pi/2$; input laser is linearly polarized. $\alpha = 0.51$ and $\alpha = \pi$ are explored. Spectra show an increasing redshift as α grows. Thin spikes represent in each case the frequency boundaries computed from analytical Doppler formula. In this figure and the following, except otherwise noted, only the emission at first harmonic is depicted for clarity.

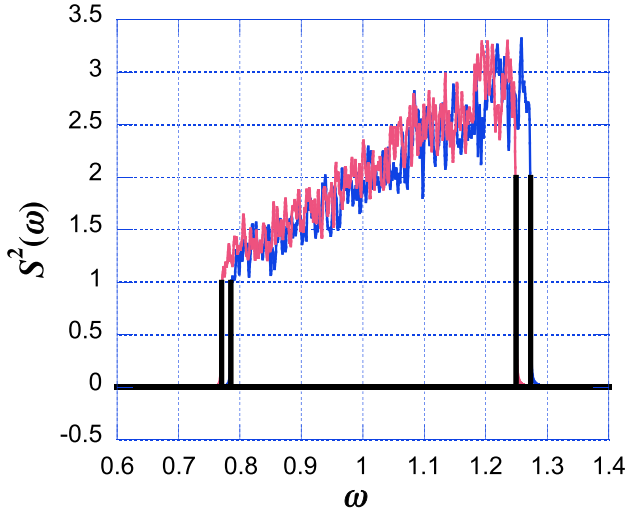

FIG. 2. Same as Figure 1, but with scattering angle $\theta_0 = \pi/4$. The main effect at hand here, apart from the α-dependent redshift, is the narrowing of spectra in forward scattering geometry, as compared with $\theta_0 = \pi/2$.

C. Power spectra per unit interval of "wave" coordinate

We shall display neatly the divergences (anticipated in Subsection II A) of the spectral energy density for the actual case of an incoming monochromatic plane wave, that is, in Eq. (25). In fact, by evaluating $|\cos\theta_0\tilde{p}_{L,1} - \sin\theta_0\tilde{p}_{L,3}|^2$ and $|\tilde{p}_{L,2}|^2$ in Eq. (25) through the use of Eqs. (28) and (27), one faces products of two Dirac delta functions, namely, $\delta(\omega g_{1,L} - l'\omega_0)\delta(\omega g_{1,L} - l''\omega_0)$. The latter product, by virtue of the properties of the Dirac delta function, vanishes for $l' \neq l''$ and equals $\delta(\omega g_{1,L} - l'\omega_0)\delta(0)$ for $l' = l''$. If one interprets the divergent $\delta(0)$ as $(2\pi)^{-1}\Delta\xi$, $\Delta\xi$ being a very large (actually, divergent) extension of the incoming monochromatic plane wave in terms of the "wave" coordinate, then the actual spectral energy density (25) diverges proportionally to $\Delta\xi$. The way to cure that divergence of the spectral energy density consists in dividing Eq. (25) by

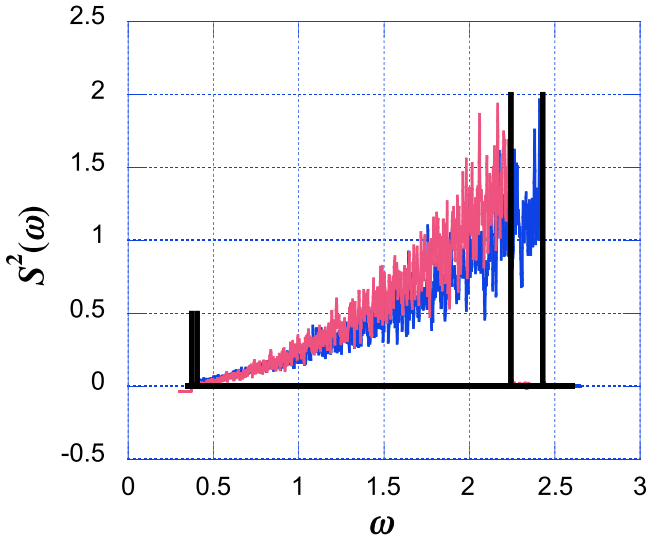

FIG. 3. Thomson scattering spectra from a monoenergetic, isotropic electron distribution function at 100 keV. $\theta_0 = \pi/2$; input laser is linearly polarized. $\alpha = 1.16$ and $\alpha = \pi$. Only the first harmonic is represented for clarity, but there is also a noticeable contribution from the second harmonic.

$\Delta\xi$, thereby introducing the power spectrum per unit intervals of solid angle, "wave" coordinate ξ and frequency.[17] That is, we consider

$$\frac{1}{\Delta\xi}\left(\frac{d^2U}{d\Omega d\omega}\right)_L \tag{32}$$

and we regard it as the physically relevant divergence-free quantity. Parenthetically, it can be seen that the first and second squared terms in Eq. (25) correspond to two orthogonal polarizations in the detector plane, the first one being the polarization along the y-axis according to the scattering geometry established in Sec. I. By using Eqs. (25), (28) and (27), the power spectrum in Eq. (32) reads

$$\begin{aligned}\frac{1}{\Delta\xi}\left(\frac{d^2U}{d\Omega d\omega}\right)_L =& \frac{F_0(mc)^2}{\omega_0^2}\sum_{l=-2}^{+2}\sum_{l'=-2}^{+2}[q^*_{L,2l}q_{L,2l'} \\ &+\cos^2\theta_0 q^*_{L,1l}q_{L,1l'} - \cos\theta_0\sin\theta_0 \\ &\times(q^*_{L,3l}q_{L,1l'} + q^*_{L,1l}q_{L,3l'}) + \sin^2\theta_0 q^*_{L,3l}q_{L,3l'}] \\ &\times\exp[i(l-l')(\pi/2)] \\ &\times\sum_{l''=-\infty}^{+\infty} J_{l+l''}(\omega_r g_{2,L}, \omega g_{3,L})J_{l'+l''}(\omega_r g_{2,L}, \omega g_{3,L}) \\ &\times\delta\left(\frac{\omega g_{1,L}}{\omega_0} - l''\right),\end{aligned} \tag{33}$$

$*$ denotes the complex conjugate. The coefficients $q_{L,jn}$ are given in Appendix B.

The formula (33) is potentially useful for the computation of Thomson scattering spectra under very general conditions regarding both the energy distribution function of the electrons and the intensity of the incoming laser. Perhaps the most difficult part (this applies to the case of ultraintense lasers, i.e., $\alpha \geq 1$) would be to fix the range of harmonics that would reasonably contribute to the spectrum for any fixed α, and, in the case of the linearly polarized wave, to evaluate the generalised Bessel functions (Appendix C) of the corresponding arguments. We plan to carry out these computations in the near future, and to compare the results and the computational efficiency of this approach with the direct integration of the equations of motion already done.[20] This applies in particular to the case of non-Maxwellian and/or anisotropic electron distribution functions (in that case, and to the best of our knowledge, analytical calculations of TS spectra being scarce), for which a large number of numerical data have been obtained from the Monte Carlo code. These results will be reported elsewhere.

D. Power spectra per unit interval of "detection" time

According to a very short statement in Ref. 17 (page 13), the power spectra per unit intervals of "detection" time (t), of solid angle and of frequency are obtained by multiplying Eqs. (44) and (33) by the same factor for both $\delta = C, L$. That factor is $F_{\mathrm{Av}} = c\gamma_1/\langle H_e\rangle$, where H_e is given in Eq. (A6) and the average $\langle\ \rangle$ is taken in a wave period. In this subsection, we shall treat the case $\delta = L$ and analyze the one

for $\delta = C$ in a subsection later. For that purpose, by using $dt = [1 - c^{-1}\mathbf{n}.(d\mathbf{x}/dt')]dt'$ (which, in turn, comes from $t' - c^{-1}\mathbf{n}.\mathbf{x}(t') = t - c^{-1}R$, $dt'/[c(\gamma_1 + p_3(\xi))] = d\xi/(c\gamma_1)$) and the first Eq. (5), one gets

$$dt = \left[1 + \frac{p_3(\xi) - \mathbf{n}.\mathbf{p}(\xi)}{\gamma_1}\right] d\xi. \tag{34}$$

As the "wave" coordinate ξ of the incoming monochromatic plane wave varies in the whole range $\Delta\xi$ (divergent), the "detection" time (t) also varies in an interval Δt (also divergent). Then, it seems natural to interpret that Δt and $\Delta\xi$ are related to one another through what will result if one integrates Eq. (34) over their whole ranges of variation

$$\Delta t = \int dt = \int \left[1 + \frac{p_3(\xi) - \mathbf{n}.\mathbf{p}(\xi)}{\gamma_1}\right] d\xi. \tag{35}$$

Notice that $\Delta\xi$ $(= \int d\xi)$ contains a very large (divergent) number of cycles for the incoming monochromatic plane wave and that $\int d\xi$ amounts to an integration over the whole electron trajectory. Equation (A8) in Appendix A shows that $\mathbf{p}(\xi)$ is independent on the choice of $\bar{A}_i$ and, hence, the same conclusion holds for Eq. (35). For simplicity, Eq. (35) for $\delta = L$ will be evaluated by choosing $\bar{A}_i(\xi)$ such that $\bar{A}_i(\xi = 0) = 0$.

The difference between Eq. (35) and F_{Av}^{-1} in Ref. 17 arises from the omission, in the latter, of the term $\mathbf{n}.\mathbf{p}(\xi)$. Recall that, for the actual incoming strictly monochromatic linearly polarized radiation, the components p_1, p_2, and p_3 of $\mathbf{p}(\xi)$ are obtained from Eqs. (3), (A4), and (A5) (or, alternatively, given in Eqs. (B.16) and (B.17) for $\delta = L$ from Ref. 20, not reproduced here, for brevity). A glance to those formulas for p_j, $j = 1, 2, 3$ show that they equal constant terms plus oscillating terms, linear in $\sin\omega_0\xi$ and $\cos 2\omega_0\xi$. It follows that $\int d\xi$ of all those oscillating terms over one cycle (and, hence, over a very large number of them) vanishes. Only the constant terms in p_j, $j = 1, 2, 3$ give a nonvanishing contribution to $\int d\xi$ in the right-hand-side of Eq. (35). Then, the latter becomes

$$\Delta t = \frac{\Delta\xi}{F_L}, \tag{36}$$

$$\frac{1}{F_L} = 1 + \frac{1 - \cos\theta_0}{\gamma_1}\left[-\frac{\gamma_1}{2} + \frac{m^2c^2}{2\gamma_1} + \frac{f_1^2 + f_2^2 + 2^{-1}(eE_0/\omega_0)^2}{2\gamma_1}\right] - \frac{f_1\sin\theta_0}{\gamma_1}. \tag{37}$$

An alternative representation for $\frac{1}{F_L}$ is given in Appendix B. One sees in Eq. (B2) (which is the counterpart of Eq. (37)) that F_L^{-1} has a quadratic dependence on α. The power spectra per unit interval of "detection" time (t) is obtained from Eq. (33) as

$$\frac{1}{\Delta t}\left(\frac{d^2U}{d\Omega d\omega}\right)_L = F_L\frac{1}{\Delta\xi}\left(\frac{d^2U}{d\Omega d\omega}\right)_L. \tag{38}$$

IV. MONOCHROMATIC CIRCULARLY POLARIZED RADIATION

A. The scalar function $b_{n,C}$ and the $\tilde{p}_{C,j}$'s

We shall now turn to the case of incoming circular polarization ($\delta = C$), for which we shall employ ($\theta = \omega_0\xi$)

$$\exp[ix\sin(\theta - \varphi)] = \sum_{l=-\infty}^{+\infty} J_l(x)\exp[il(\theta - \varphi)], \tag{39}$$

which, in turn, follows from the generating function for the $J_l(z)$'s and its associated series.[24] Then, by integrating over ξ and using Dirac's delta function in Eq. (24), one gets the counterpart of Eq. (27) ($\omega_r = \omega/\omega_0$)

$$b_{n,C} = \frac{(2\pi)^{1/2}}{\omega_0}\exp[i\omega_r g_{0,C}]\sum_{l'=-\infty}^{+\infty} J_{-l'-n}(\omega_r g_{2,C}) \times \exp[i(n + l')\varphi_C]\delta(\omega_r g_{1,C} - l'). \tag{40}$$

For brevity, we do not enter here into a discussion of the signs and values of φ_C. One has

$$\tilde{p}_{C,j} = mc\sum_{n=-1}^{+1} q_{C,jn}b_{n,C}, \quad j = 1, 2, 3. \tag{41}$$

The coefficients $q_{C,jn}$ are dimensionless. Their detailed expressions in terms of the laser parameter, etc. are given in Appendix B. The algebraic computations yielding Eq. (41) make use of Eqs. (4), (A4), and (A5) (or, alternatively, of Eqs. (B.21) and (B.22) for $\delta = C$ from Ref. 20, not reproduced here, for brevity).

B. Doppler-like formulas: Laser-parameter dependence

Like for Eq. (27), one realizes that the only nonvanishing contributions to $b_{n,C}(\mathbf{y}, \omega)$ (by virtue of the δ's in Eq. (40) are obtained for scattered frequencies $\omega = \omega_{C,l'}$ that fulfill the generalized Doppler-like formula for circularly polarized incident radiation

$$\omega_{C,l'} = \frac{l'\omega_0}{g_{1,C}} = \frac{l'\omega_0[1 - \beta_{03}]}{1 - \mathbf{n}_0.\boldsymbol{\beta}_0 + (1 - \cos\theta_0)\left[\frac{1 - \boldsymbol{\beta}_0^2}{1 - \beta_{03}}\right]\left[\left(\frac{\alpha}{2\pi}\right)^2 + \left(\frac{\alpha}{2\pi}\right)\frac{\beta_{02}}{(1 - \boldsymbol{\beta}_0^2)^{1/2}}\right]} \tag{42}$$

for the given $g_{1,C}$ (see Eq. (20)) and for all the integers l' $(= 0, \pm 1, \pm 2, \pm 3, ...)$. Some general comments made on Eq. (29) for linearly polarized radiation also apply for Eq. (42). For instance, for small α, only the harmonic with $l' = 1$ will contribute to the spectrum but, as α grows, power will be found at higher harmonics ($l' > 1$), consistently with Ref. 20. Equation (42) does depend on the laser parameter and on the fact that circularly polarized laser radiation is now considered. We emphasize the differences between Eqs. (30) and (42): (i) the coefficient of α^2 is different in them (but see comments below) and (ii) Eq. (42) contains an additional term linear in α, and proportional to β_{02} as well. The generalized Doppler formulas (30) and (42) predict a redshift of the scattered frequency for very intense laser radiation and also predict that the fine details of this redshift be different for linear and circular polarization. In fact, if the linear term proportional to β_{02} in Eq. (42) is small, the only difference between both cases will be the factor $\alpha/4\pi$ for linear polarization vs. $\alpha/2\pi$ for circular polarization, which we think is a consequence of the fact that the *power* of a circularly polarized wave of a maximum electric field equal to E_0 is *twice* as large as the input power of a linearly polarized wave of peak electric field equal to E_0. That means that $\alpha/2$ should be used for the case of a circularly polarized wave when comparing formulas (30) and (42). With the above understanding, the only difference between them comes from the term proportional to β_{02}, which is present for circular polarization, but absent for linear polarization, and the equations can be conveniently cast as ($\gamma_0 = [1 - \boldsymbol{\beta}_0^2]^{-1/2}$)

$$\omega_{C,l'} = l'\omega_0 \times \frac{1 - \beta_{03}}{1 - \mathbf{n}_0.\boldsymbol{\beta}_0 + \frac{\alpha}{4\pi\gamma_0}(1 - \cos\theta_0)\left[\frac{\alpha}{4\pi\gamma_0} + \beta_{02}\right]\Big/(1 - \beta_{03})}. \tag{43}$$

A quantitative comparison with the Monte Carlo computations in Ref. 20 regarding overall redshifts in scattered spectra for ultraintense lasers has also been made for circular polarization, which confirms that redshift. A systematic check of the Doppler formula for circular polarizations has been made, for monoenergetic and isotropic electron distribution functions of 25 keV and 100 keV, and for several values of the α parameter and the scattering angle θ_0. The comparison between the bounds predicted by Doppler formulas and the numerical computations has always been excellent, with small (but noticeable nonetheless) differences between linear and circular polarizations. In one case, a monoenergetic but *anisotropic* electron distribution function has been considered, enhancing the contribution of the β_{02} term (at 25 keV). The anisotropic electron distribution function has been chosen as follows: electrons are emitted uniformly into a cone of semiaperture $= 10^\circ$, the axis of the cone being defined by $\theta = \pi/2$ and $\varphi = \pi/4$. In that case, agreement theory/computation is also excellent, but on top of this, the different predictions of Doppler formulas related with the polarization of the input wave are brought clearly into focus; see Figures 4 and 5 below for further details.

It is important to compare Eq. (42) with a generalized Doppler formula obtained by Avetissian for both linearly and circularly polarized incident radiation (recall that the comparison of the latter with Eq. (30), for linearly polarized radiation, was discussed above). After some amount of algebraic computation, one can show that our Eq. (42) for circularly polarized incident radiation disagrees from Avetissian's generalized formula in Ref. 17. In fact, while Avetissian obtains the same generalized Doppler formula for both linearly and circularly polarized incident radiation (and so, with a quadratic dependence on the laser parameter), our Eq. (42) displays a dependence on the laser parameter, which is both quadratic and linear.

Equations (30) and (42) have been obtained by choosing, for simplicity, $\bar{A}_i(\xi)$ such that $\bar{A}_i(\xi = 0) = 0$. The analysis in Appendix A (Eq. (A8)) implies that Eqs. (30) and (42) are independent on the choice of $\bar{A}_i$. We shall discuss relationships to other Doppler-like formulas at the end of Appendix A.

C. Power spectra per unit interval of "wave" coordinate

The analysis of the power spectra per unit interval of "wave" coordinate for incoming monochromatic circularly polarized radiation is entirely analogous to that for linearly polarized radiation, provided that use be made now of Eqs. (25), (41), and (40). Then, the power spectrum in Eq. (32) reads, for $\delta = C$ and per unit interval of "wave" coordinate

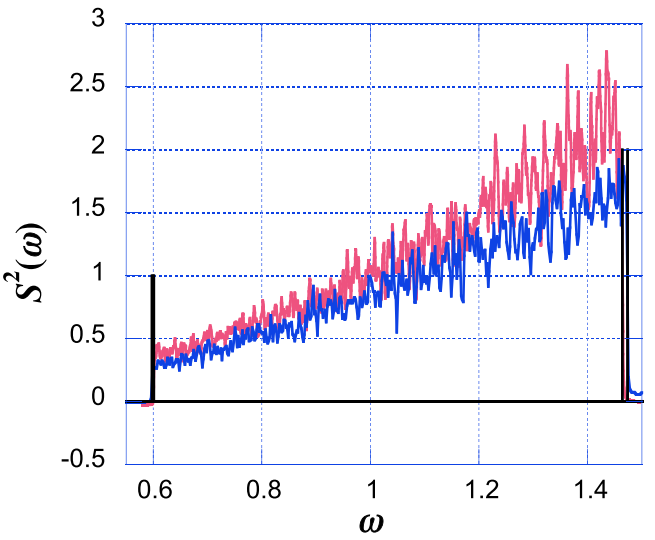

FIG. 4. Thomson scattering spectra from a monoenergetic, isotropic electron distribution function at 25 keV, $\theta_0 = \pi/2$ and two different laser polarizations, linear (red curve) and circular (blue curve). $\alpha = \pi$. Small but discernible differences between both cases are observed. Frequency boundary limits given by Doppler formulas are in excellent agreement with the numerical computation.

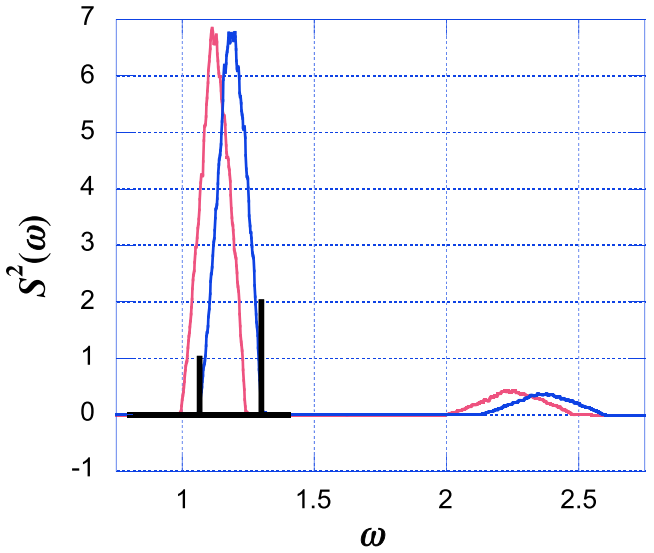

FIG. 5. Thomson scattering spectra from a monoenergetic but anisotropic (see main text for details) electron distribution function at 25 keV, $\theta_0 = \pi/2$ and two different laser polarizations, linear (blue curve) and circular (red curve). $\alpha = \pi$. The anisotropy of the distribution function makes that all the electrons have a substantial β_{02} component, enhancing the difference between both cases. Thin spikes marking boundary limits are shown, for the sake of clarity, only for the case of linear polarization. The contribution of the second harmonic has been highlighted in this figure.

$$\frac{1}{\Delta\xi}\left[\frac{d^2U}{d\Omega d\omega}\right]_C = \frac{F_0(mc)^2}{\omega_0^2}\sum_{l=-1}^{+1}\sum_{l'=-1}^{+1}[q^*_{C,2l}q_{C,2l'} + \cos^2\theta_0 q^*_{C,1l}q_{C,1l'} - \cos\theta_0\sin\theta_0 \times (q^*_{C,3l}q_{C,1l'} + q^*_{C,1l}q_{C,3l'}) + \sin^2\theta_0 q^*_{C,3l}q_{C,3l'}] \times \exp[i(-l+l')\varphi_C] \times \sum_{l''=-\infty}^{+\infty} J_{-l-l''}(\omega_r g_{2,C})J_{-l'-l''}(\omega_r g_{2,C}) \times \delta\left(\frac{\omega g_{1,C}}{\omega_0} - l''\right). \quad (44)$$

The coefficients $q_{C,jn}$ are given in Appendix B.

D. Power spectra per unit interval of "detection" time

The analysis of the power spectra per unit interval of "detection" time for circularly polarized radiation is entirely analogous to that for linearly polarized one, provided that use now be made of Eqs. (25), (41), and (40) and the counterpart of Eq. (35) for circular polarization. Recall that, for the actual incoming strictly monochromatic radiation, the components p_1, p_2, and p_3 of $\mathbf{p}(\xi)$ are obtained from Eqs. (4), (A4), and (A5) (or, alternatively, given in Eqs. (B.21) and (B.22) for $\delta = C$ from Ref. 20, not reproduced here, for brevity). A glance to those formulas for p_j, $j = 1, 2, 3$ show that they equal constant terms plus oscillating terms, linear in $\sin\omega_0\xi$, $\cos\omega_0\xi$ and $\cos 2\omega_0\xi$. As for $\delta = L$, only the constant terms in p_j, $j = 1, 2, 3$ give a nonvanishing contribution to $\int d\xi$ in the actual Δt. Then,

$$\Delta t = \frac{\Delta\xi}{F_C}, \quad (45)$$

$$\frac{1}{F_C} = 1 + \frac{1-\cos\theta_0}{\gamma_1}\left[-\frac{\gamma_1}{2} + \frac{m^2c^2}{2\gamma_1} + \frac{f_1^2 + (f_2 + (eE_0/\omega_0))^2 + (eE_0/\omega_0)^2}{2\gamma_1}\right] - \frac{f_1\sin\theta_0}{\gamma_1}. \quad (46)$$

For simplicity, Eq. (46) for $\delta = C$ has been obtained by choosing $\bar{A}_i(\xi)$ such that $\bar{A}_i(\xi = 0) = 0$. An alternative representations for $\frac{1}{F_C}$ is given in Appendix B.

Our analysis shows that differences arise between the cases $\delta = C$ and $\delta = L$. One sees in Eqs. (B1) and (B2) (which are the counterparts of Eqs. (46) and (37), respectively) that F_C^{-1} contains a dependence on the laser parameter (α), which is both quadratic and linear, while F_L^{-1} has only a quadratic dependence on α. A similar difference regarding the corresponding Doppler-like frequencies in Eqs. (42) and (30) was remarked above. The difference between the counterpart of Eq. (35) for $\delta = C$ and F_{Av}^{-1} in Ref. 17 arises from the omission, in the latter, of the term $\mathbf{n}.\mathbf{p}(\xi)$. Such an omission will give rise to the differences between Eq. (46) ($\delta = C$) and Eq. (37) ($\delta = L$).

The power spectra per unit interval of "detection" time (t) for $\delta = C$ is now obtained by multiplying Eq. (44) by F_C

$$\frac{1}{\Delta t}\left(\frac{d^2U}{d\Omega d\omega}\right)_C = F_C\frac{1}{\Delta\xi}\left(\frac{d^2U}{d\Omega d\omega}\right)_C. \quad (47)$$

V. POWER SPECTRA: QUADRATIC BEHAVIOR IN FREQUENCY AND REDSHIFT

Equation (11) contains an overall ω factor in the general case, arising from a partial integration. Such a factor gives rise to an overall ω^2 factor, in turn, in Eqs. (33) and (44) (through the factor F_0 in Eq. (17)) for the TS spectral power per unit solid angle and per unit intervals of "wave" coordinate and frequency. From this, it follows that the TS power spectra per unit solid angle and per unit intervals of "detection" time and frequency in Eqs. (38) and (47) also contain the factor ω^2. This, in turn, justifies that the power spectra of the monoenergetic electron distribution behaves as the square of the Doppler-shifted scattered frequency approximately, for electron energies up to about 400 keV and low intensity lasers, as obtained numerically in Ref. 20.

For given $\boldsymbol{\beta}_0$ and $\mathbf{n}_0$, the denominators in both Eqs. (30) and (42) increase as the laser parameter α increases. The denominator in Eq. (30) increases as α^2. Due to the linear term in α, the increase of the denominator in Eq. (42) goes like α^2 only for adequately large α. Then if l' is also fixed, the right-hand-sides of both Eqs. (30) and (42) decrease as the laser parameter increases. Then, it follows that the TS power spectra per unit "wave" coordinate and per unit "detection" time for both linearly and circularly polarized radiations are both redshifted for increasingly larger values of the laser parameter, as also obtained numerically in Ref. 20.

VI. CONCLUSIONS AND FINAL COMMENTS

Here, we have presented an analytical justification of the quadratic behavior in frequency and redshift of the power

spectra, obtained numerically in our previous work:[20] see Sec. V above. Those justifications have been carried out by extending suitably analytical approaches, as developed by other authors. Moreover, our analytical treatment exhibits differences between the Doppler-like frequencies for linear and circular polarization of the incoming radiation, which do not appear to have been displayed by previous authors. We have proved that the Doppler-like frequencies (Eqs. (30) and (42)) are independent on the choice of gauge of the potential vector ($\bar{A}_i$), as physically expected.

We emphasize three important differences between the treatment in Ref. 17 and the one here. First, in our analysis of the spectral asymptotic Liénard-Wiechert retarded radiation, we allow for the possibility that $\boldsymbol{\beta}_0.\mathbf{A}_i$ be either $= 0$ or $\neq 0$. Second, and consequently, we have arrived at the structures dependent on both $\boldsymbol{\beta}_0$ and on α in the denominators of both Eqs. (30) and (42). Equation (30) contains a α^2-dependence and is consistent with the generalized Doppler formula obtained in Ref. 17. On the other hand, the structure of Eq. (42) displays dependences on both α and α^2 and, so it differs from the formula in Ref. 17 (which only contains α^2). Those differences in the Doppler-like frequencies for linear and circular polarization are validated by new Monte Carlo computations, reported here. Third, we have obtained the TS power spectra per unit interval of the "detection" time t for incoming monocromatic plane wave radiations and displayed the differences for circular and linear polarizations: see Eqs. (46) and (37). Those TS spectra are consistent with Monte Carlo results for the regimes considered in Ref. 20 and, hence, not reproduced here.

The analytical expressions obtained for the scattered spectrum are given in terms of infinite series of Bessel functions (circular polarization) and of the so-called generalised Bessel functions (linear polarization). We have cast these expressions into forms more suitable for efficient computation. A particularly useful aspect, among others, is that we have presented all the relevant variables in dimensionless form, so as to bring the different parametric dependences clearly into focus.

We have analyzed how the generalized Doppler formulas (30) and (42) would be modified for a general incoming non-monochromatic plane-wave. In that case, the dependence of $\Lambda(\xi)$ (Eq. (15)) on ξ is more complicated than the one displayed in Eq. (18), for both linear and circular polarizations. Then, for an incoming non-monocromatic plane wave radiation, $\tilde{\mathbf{p}}(\mathbf{y},\omega)$ in Eq. (13) will not contain in general Dirac delta functions displaying exactly Doppler-like formulas like those in Eqs. (40) and (27) for incoming strictly monochromatic radiation. We omit further details.

The analytical treatment presented in this work is planned to be checked against the results of the Monte Carlo code on new grounds: In particular, the TS spectra arising from non-Maxwellian or anisotropic electron distribution functions.

ACKNOWLEDGMENTS

R. F. Álvarez-Estrada acknowledges Ministerio de Ciencia e Innovación, Spain, for financial support under Project FIS2008-01323. F. Castejón and I. Pastor also acknowledge Ministerio de Ciencia e Innovación, Spain, for financial support under Projects ENE2008-06082/FTN and ENE2009-10181, respectively. R. F. Álvarez-Estrada and F. Castejón are associate members of Instituto de Biocomputación y Física de los Sistemas Complejos, Universidad de Zaragoza, Zaragoza, Spain.

APPENDIX A: SOLUTION OF EQ. (5) AND DISCUSSION

The exact solution of Eq. (5), with $\mathbf{E} = \mathbf{E}_i$ and $\mathbf{B} = \mathbf{B}_i$, when the input $\mathbf{A}_i$ describes the general non-monochromatic plane wave outlined in Subsection I A, has been given in Ref. 12 (Chapter 6, Section 47, Problem 2), by solving exactly the associated Hamilton-Jacobi equation. That general solution has been also discussed in Ref. 13 and it has been summarized,[20] in a way suitable for our purposes. For other studies of that solution, see Refs. 14–18. Here, we shall employ end extend our previous treatment.[20] Thus, the general solutions of Eq. (5), with those $\mathbf{E}_i$ and $\mathbf{B}_i$ are $\mathbf{x} = (\bar{x}, x_3) = (x_1, x_2, x_3)$ and $\mathbf{p} = (\bar{p}, p_3) = (p_1, p_2, p_3)$, which contain six suitable integration constants. Recall that variables with overbars are two-dimensional vectors in the (y_1, y_2)-plane. Let $\mathbf{P}(= \mathbf{P}(t))$ be the generalized three momentum, at time t. One has $\mathbf{p} = \mathbf{P} - e\mathbf{A}_i$. We write the general solution as

$$\bar{x}(\xi) = \bar{x}_0 + \frac{c\xi\bar{f}}{\gamma_1} - \frac{ec}{\gamma_1}\int_0^\xi d\xi' \bar{A}_i(\xi'), \tag{A1}$$

$$x_3(\xi) = x_{3,0} + s\xi + \frac{c}{2\gamma_1^2}\int_0^\xi d\xi' [-2e\bar{f}\bar{A}_i(\xi') + e^2\bar{A}_i(\xi')^2], \tag{A2}$$

$$s = \frac{m^2c^3 + c\bar{f}^2}{2\gamma_1^2} - \frac{c}{2}, \tag{A3}$$

$$\bar{P} = \bar{f}, \quad \bar{p}(\xi) = \bar{f} - e\bar{A}_i(\xi), \tag{A4}$$

$$P_3(\xi) = -\frac{\gamma_1}{2} + \frac{m^2c^2}{2\gamma_1} + \frac{(\bar{f} - e\bar{A}_i(\xi))^2}{2\gamma_1} = p_3(\xi). \tag{A5}$$

It is understood that, in Eqs. (A1), (A2) and (A4), (A5), one sets $\xi = t - x_3/c$ which, together with Eq. (A2), justify to regard the present exact solution as an implicit one. The six integration constants are: $\bar{x}_0 = (x_{0,1}, x_{0,2})$ and $x_{3,0}$ (the three-dimensional vector determining the position of the electron at $\xi = 0$), $\bar{f} = (f_1, f_2)$ (the ξ-independent two-dimensional generalized momentum of the electron), and γ_1. γ_1 has the physical dimension of momentum and, then, it should not be confused with the standard dimensionless $\gamma(t)$ appearing in Eq. (5). More about γ_1 will be summarized below. The integration of Eq. (5) through the method in Ref. 12 gives, in the solution for $x_3(\xi)$ in Eq. (A2), a fraction involving integration constants, which is denoted here as s (Eq. (A3)), for the sake of compactness. Notice that $\bar{x}(\xi = 0) = 0$ and $x_3(\xi = 0) = 0$. The alert reader could well ask why Eqs. (A1), (A2) and (A4), (A5) contain powers of $\bar{A}_i$ not higher than two. The reason is that the solution in Eqs. (A1)–(A5) is

simple only in an apparent sense, while it is intrinsically implicit and highly nonlinear. In fact, by replacing x_3 in $\xi = t - x_3/c$ by the right-hand-side of Eq. (A2), solving iteratively to get $\xi = \xi(t)$ and reshuffing the latter into Eqs. (A1), (A2), (A4), and (A5), one would get any power of the vector potential $\bar{A}_i$ higher than two. Then, (infinite) subsets of terms in the resulting intrinsically highly nonlinear solution for $\bar{x}$, x_3, $\bar{p}$, and p_3, generated through the above iterative procedure, could well be equivalent to (or show up as) new structures not explicitly displayed in Eqs. (A1), (A2) and (A4), (A5): for instance, the standard γ (depending on $\bar{A}_i$).

The total energy of the electron, subject only to the incoming electromagnetic field (having omitted the dynamical field) is

$$H_e = [m^2c^4 + c^2\mathbf{p}^2]^{1/2}. \tag{A6}$$

Since $\mathbf{p}$ is not constant, it follows that $H_e = H_e(\xi)$, so that Eq. (A6) does not express any sort of quasi-static approximation, but a dynamical one (namely, that in the framework of the approximation scheme in Subsection I B. By using Eq. (5), it is straightforward to show that $H_e(\xi) - cp_3(\xi)$ is a constant of motion. On the other hand, some direct algebraic manipulations with Eqs. (A4)–(A6) shows that

$$H_e = c[\gamma_1 + p_3(\xi)]. \tag{A7}$$

It then follows that the integration constant γ_1 is also a constant of motion. The components of $\bar{x}_0$ and of $\bar{f}$ and $x_{3,0}$ are allowed to vary in $(-\infty, +\infty)$. We shall always take $\gamma_1 \geq 0$. There are three regimes for $e = 0$: $0 \leq \gamma_1 < +[m^2c^2 + \bar{f}^2]^{1/2}$ (with $+\infty > s > 0$), $\gamma_1 = [m^2c^2 + \bar{f}^2]^{1/2}$ (with $s = 0$), and $+\infty > \gamma_1 \geq [m^2c^2 + \bar{f}^2]^{1/2}$ (with $-(c/2) \leq s < 0$).

The electromagnetic field corresponding to the incoming laser radiation is described by unique electric and magnetic fields ($\mathbf{E}_i$ and $\mathbf{B}_i$), and physical phenomena and magnitudes determined by the latter (like the dynamics and trajectory of the relativistic electron) are also uniquely determined. On the other hand, the choice of the potential vector $\mathbf{A}_i$ or $\bar{A}_i$ is not unique: thus the transformation $\bar{A}_i(\xi) \to \bar{A}_i{}'(\xi) = \bar{A}_i(\xi) + \delta\bar{A}_i$, $\delta\bar{A}_i$ being independent on ξ, gives rise to the same $\mathbf{E}_i$ and $\mathbf{B}_i$. All that is a restriction to the actual case of the well known gauge invariance of the electromagnetic field. A glance at Eqs. (A1)–(A5) indicates that they depend on $\bar{A}_i$ and, hence, the question whether the former are uniquely determined arises, to which we now turn. Let us consider the solution $\bar{x}$, x_3, $\bar{p}$, and p_3 given in Eqs. (A1) and (A2), (A4) and (A5), and (A3), with $\bar{A}_i$ and s and integration constants γ_1, $\bar{x}_0 = (x_{0,1}, x_{0,2})$, $x_{3,0}$ and $\bar{f} = (f_1, f_2)$. Let $\bar{x}'$, $x_3{}'$, $\bar{p}'$, and $p_3{}'$ be another solution, also given by Eqs. (A1) and (A2), (A4) and (A5), and (A3), now with a new $\bar{A}_i{}'$, the same integration constants γ_1, $\bar{x}_0 = (x_{0,1}, x_{0,2})$, and $x_{3,0}$ but with other integration constants $\bar{f}' = (f_1{}', f_2{}') (\neq \bar{f})$ which, in turn, determines a new s' (in order to have a consistent description). Let $\bar{A}_i(\xi)$ and $\bar{A}_i{}'(\xi)$ be related by the (gauge) transformation, $\bar{A}_i(\xi) \to \bar{A}_i(\xi) + \delta\bar{A}_i = \bar{A}_i{}'(\xi)$, $\bar{f} \to \bar{f}' = \bar{f} + e\delta\bar{A}_i$ and $s \to s' = s + c[e^2\delta\bar{A}_i^2 + 2e(\bar{f}\,\delta\bar{A}_i)]/(2\gamma_1^2)$, $\delta\bar{A}_i$ being ξ-independent. Some algebra shows that (for ξ)

$$\bar{x}' = \bar{x}, \quad x_3{}' = x_3, \quad \bar{p}' = \bar{p}, \quad p_3{}' = p_3, \tag{A8}$$

for any ξ-independent $\delta\bar{A}_i$. Equation (A8) prove that the dynamics and trajectory of the relativistic electron are independent on the choice of $\delta\bar{A}_i$.

The above solution is rather complicated due, in particular, to the dependence on the variable ξ and on $e\bar{A}_i(\xi) \neq 0$ and, so a more specific analysis appears to be adequate. For that purpose, we shall consider a general plane-wave with incoming wavevector along $\mathbf{k} = (0, 0, 1)$ (the unit vector along the y_3 axis) expressed as

$$\bar{A}_i = \bar{A}_i(\xi) = \mathbf{i}c_\delta\left[-\sum_l \frac{E_{0.l}}{\omega_{0,l}}\sin\omega_{0,l}\xi\right] + \mathbf{j}\left[(1-c_\delta) \times\left(-\sum_l \frac{E_{0.l}}{\omega_{0,l}}\sin\omega_{0,l}\xi\right) + c_\delta\sum_l \frac{E_{0.l}}{\omega_{0,l}}(\cos\omega_{0,l}\xi - 1)\right] \tag{A9}$$

with real amplitudes $E_{0,l}$ and real frequencies $\omega_{0,l}$. Both the index δ and the coefficient c_δ have the same meaning as in Subsection II B: they enable to treat either linear ($\delta = L$) or circular ($\delta = C$) polarization in a compact way. l and $\sum_l$ constitute a purely formal notation, which embodies both the case of discretized frequencies (l being, then, a discrete index: $l = 1, 2, 3, \ldots$, varying in a finite or denumerably infinite range), and the case of a continuous distribution of frequencies ($\omega_{0,l} \to \omega_0$, which is a continuous real variable, with $\sum_l \to (\Delta\omega)^{-1}\int_{\omega_{0,m}}^{\omega_{0,M}} d\omega_0$, $\omega_{0,m}$ and $\omega_{0,M}$ being the lower and upper frequency limits, with a suitable normalizing frequency interval $\Delta\omega$), and $E_{0,l} \to E_0(\omega_0)$. Notice that $\bar{A}_i(\xi = 0)$ vanishes, which amounts to a definite choice of gauge.

We use Eq. (A9) into Eqs. (A1) and (A2). After performing the integrations, we get

$$x_1 = x_{0,1} + \frac{cf_1\xi}{\gamma_1} + \frac{c_\delta ce}{\gamma_1}\sum_l \frac{E_{0.l}}{\omega_{0,l}^2}[1 - \cos\omega_{0,l}\xi], \tag{A10}$$

$$x_2 = x_{0,2} + \frac{cf_2\xi}{\gamma_1} + \frac{ce}{\gamma_1}\left[(1-c_\delta)\sum_l \frac{E_{0.l}}{\omega_{0,l}^2}(1 - \cos\omega_{0,l}\xi) - c_\delta\sum_l \frac{E_{0.l}}{\omega_{0,l}}\left(-\xi + \frac{\sin\omega_{0,l}\xi}{\omega_{0,l}}\right)\right], \tag{A11}$$

$$x_3 = x_{3,0} + s\xi + x_{3,1} + x_{3,2} + x_{3,3}, \tag{A12}$$

$$x_{3,1} = \frac{ce}{\gamma_1^2}\left[(f_1c_\delta + f_2(1-c_\delta))\sum_l \frac{E_{0.l}}{\omega_{0,l}^2}(1 - \cos\omega_{0,l}\xi) - f_2c_\delta\sum_l \frac{E_{0.l}}{\omega_{0,l}}\left(-\xi + \frac{\sin\omega_{0,l}\xi}{\omega_{0,l}}\right)\right], \tag{A13}$$

$$x_{3,2} = \frac{ce^2}{2\gamma_1^2}\sum_l \frac{E_{0.l}}{\omega_{0,l}}\sum_{l'} \frac{E_{0.l'}}{\omega_{0,l'}}\left[\frac{\sin(\omega_{0,l} - \omega_{0,l'})\xi}{2(\omega_{0,l} - \omega_{0,l'})} - \frac{\sin(\omega_{0,l} + \omega_{0,l'})\xi}{2(\omega_{0,l} + \omega_{0,l'})}\right], \tag{A14}$$

$$x_{3,3}=\frac{ce^2c_\delta^2}{2\gamma_1^2}\sum_l\frac{E_{0.l}}{\omega_{0,l}}\sum_{l'}\frac{E_{0.l'}}{\omega_{0,l'}}\Big[\xi-\frac{\sin\omega_{0,l}\xi}{\omega_{0,l}}-\frac{\sin\omega_{0,l'}\xi}{\omega_{0,l'}}+\frac{\sin(\omega_{0,l}+\omega_{0,l'})\xi}{2(\omega_{0,l}+\omega_{0,l'})}+\frac{\sin(\omega_{0,l}-\omega_{0,l'})\xi}{2(\omega_{0,l}-\omega_{0,l'})}\Big], \tag{A15}$$

p_1, p_2 and p_3 are given directly in terms of ξ through Eqs. (A4) and (A5) and Eq. (A9). We shall now apply Eqs. (A10)–(A12) to an incoming narrow pulse. $\Delta\omega_0\simeq\delta\omega(>0)$ is suitably small, so that we approximate $E_0(\omega_0)\simeq E_0(\omega_{0,1})\equiv E_{0,1}$ and $\omega_0^{-n}\simeq\omega_{0,1}^{-n}$, $n=1,2\ldots$ Let

$$\Lambda_1=\int_{-\delta\omega}^{+\delta\omega}\frac{du}{2\delta\omega}\frac{\sin u\xi}{u\xi},\quad \Lambda_2=\frac{\sin(\xi\delta\omega/2)}{(\xi\delta\omega/2)}. \tag{A16}$$

After the above approximations and some computations, Eqs. (A10)–(A12) become

$$x_1=x_{0,1}+\frac{cf_1\xi}{\gamma_1}+\frac{c_\delta ce}{\gamma_1}\frac{E_{0.1}}{\omega_{0,1}^2}[1-\Lambda_2\cos\omega_{0,1}\xi], \tag{A17}$$

$$x_2=x_{0,2}+\frac{cf_2\xi}{\gamma_1}+\frac{ce}{\gamma_1}\Big[(1-c_\delta)\frac{E_{0.1}}{\omega_{0,1}^2}(1-\Lambda_2\cos\omega_{0,1}\xi)-c_\delta\frac{E_{0.1}}{\omega_{0,1}}\Big(-\xi+\Lambda_2\frac{\sin\omega_{0,1}\xi}{\omega_{0,1}}\Big)\Big], \tag{A18}$$

$$x_3=x_{3,0}+s\xi+x_{3,1}+x_{3,2}+x_{3,3}, \tag{A19}$$

$$x_{3,1}=\frac{ce}{\gamma_1^2}\Big[(f_1c_\delta+f_2(1-c_\delta))\frac{E_{0.1}}{\omega_{0,1}^2}(1-\Lambda_2\cos\omega_{0,1}\xi)-f_2c_\delta\frac{E_{0.1}}{\omega_{0,1}}\Big(-\xi+\Lambda_2\frac{\sin\omega_{0,1}\xi}{\omega_{0,1}}\Big)\Big], \tag{A20}$$

$$x_{3,2}=\frac{ce^2}{2\gamma_1^2}\frac{E_{0.1}^2}{\omega_{0,1}^2}\Big[\frac{\Lambda_1\xi}{2}-\Lambda_2\cos(\xi\delta\omega/2)\frac{\sin(2\omega_{0,1}\xi)}{4\omega_{0,1}}\Big], \tag{A21}$$

$$x_{3,3}=\frac{ce^2c_\delta^2}{2\gamma_1^2}\frac{E_{0.1}^2}{\omega_{0,1}^2}\Big[\xi-\frac{2\Lambda_2\sin\omega_{0,1}\xi}{\omega_{0,1}}+\frac{\Lambda_1\xi}{2}+\Lambda_2\cos(\xi\delta\omega/2)\frac{\sin(2\omega_{0,1}\xi)}{4\omega_{0,1}}\Big]. \tag{A22}$$

For consistency, let us now consider an incoming strictly monocromatic plane wave, either linearly or circularly polarized. Then, one has $\delta\omega\to 0$ and, hence, $\Lambda_1\to 1$ and $\Lambda_2\to 1$, and let us write $E_{0,1}\equiv E_0$ and $\omega_{0,1}\equiv\omega_0$. Let us now consider an incoming linearly polarized strictly monocromatic plane wave ($c_{\delta=L}=0$): recall Eq. (3). Then, Eqs. (A17)–(A19) become correctly Eqs. (B.13) and (B.14) in Ref. 20. Notice that in Ref. 20, instead of ξ, we employed $\Phi=\omega_0\xi$. On the other hand, there is a small missprint in Eq. (B.15) in Ref. 20 for a linearly polarized strictly monocromatic plane wave (which did not affect the extensive numerical computations there at all). The correct equation corresponding to Eq. (B.15) in Ref. 20 (and hence free of that missprint) is

$$x_3=x_{3,0}+s\xi+\frac{c}{2\gamma_1^2}\frac{2eE_0f_2(1-\cos\xi\omega_0)}{\omega_0^2}+\frac{c}{2\gamma_1^2}\frac{(eE_0)^2}{4\omega_0^3}[2\omega_0\xi-\sin(2\omega_0\xi)]. \tag{A23}$$

For an incoming circularly polarized strictly monocromatic plane wave with $c_{\delta=C}=1$ (Eq. (4)). Then, Eqs. (A17)–(A19) yield correctly Eq. (B.18) in Ref. 20 On the other hand, there are two small misprints in Eqs. (B.19) and (B.20) in Ref. 20 for a circularly polarized strictly monocromatic plane wave (which did not affect either the extensive numerical computations there at all). The correct equations corresponding to Eqs. (B.19) and (B.20) in Ref. 20 (and hence free of those missprints) are

$$x_2=x_{0,2}+\Big[\frac{cf_2}{\gamma_1}+\frac{ceE_0}{\gamma_1\omega_0}\Big]\xi-\frac{ceE_0\sin\omega_0\xi}{\gamma_1\omega_0^2}, \tag{A24}$$

$$x_3=x_{3,0}+\Big[s+\frac{ceE_0[f_2+(eE_0)/\omega_0]}{\gamma_1^2\omega_0}\Big]\xi-\frac{ceE_0}{\gamma_1^2\omega_0^2}\times[f_1(-1+\cos\omega_0\xi)+(f_2+(eE_0/\omega_0))\sin\omega_0\xi]. \tag{A25}$$

The exact solutions have been very useful for comparisons with the numerical solutions in Ref. 20, for the purely monochromatic case. In the latter and for both linearly and circularly polarized cases, we used the following initial conditions at $t=0$: $x_{0,1}=x_{0,2}=x_{3,0}=0$, f_1, f_2 and (as the sixth initial condition) either γ_1 or $p_3(\xi=0)$ or the electron initial energy $c[\gamma_1+P_3(\xi=0)]=mc^2[1-\boldsymbol{\beta}_0^2]^{-1/2}$ ($f_i=mc\beta_{0i}[1-\boldsymbol{\beta}_0^2]^{-1/2}$, and $i=1,2$).

Let us return to Eqs. (A17)–(A19) (narrow pulse) and use them into Eqs. (13) ($\tilde{\mathbf{p}}(\mathbf{y},\omega)$) and (15) ($\Lambda(\xi)=\Lambda(\xi)_\delta$). Then, one readily finds that Eq. (15) cannot give rise to Dirac delta functions ($\delta(\omega_r g_{1,\delta}-l')$) like those in Eqs. (40) and (27), precisely due to Λ_1 and Λ_2. For a narrow pulse, one does not arrive at Doppler-like formulas like Eq. (30) and (42). This negative result is in contrast with the Doppler-like formulas obtained in Refs. 14 and 15. We also remark that the Doppler-like formulas obtained in Refs. 14 and 15 for linear and circular polarizations appear to coincide with each other. Pulses were considered in Refs. 14 and 15. We attribute those features to the different kinds of approximations for pulses carried out in Refs. 14 and 15 and in the present work.

APPENDIX B: FORMULAS USING DIMENSIONLESS COEFFICIENTS

Let us collect here conventions and notations to be used in this Appendix. We shall keep $x_{0,1}$, $x_{0,2}$, and $x_{3,0}$ throughout the formulas (although, without loss of generality, they have been set equal to 0 in the numerical computations, as indicated in Appendix A). θ_0 and α are the scattering angle and the laser parameter, respectively, as defined in Sec. I. Equation (A8) in Appendix A show that the electron trajectory and dynamics are independent on the choice of $\bar{A}_i$. The equations in this Appendix will be based upon the following choice for $\bar{A}_i(\xi)$

of the monochromatic plane wave: $\bar{A}_i(\xi=0)=0$. A subscript n in a variable will indicate that the latter is dimensionless (after having scaled it suitably). For example, for the initial position and relativistic momentum of the electron $x_{n,0,1}=x_{0,1}/\lambda$, $x_{n,0,3}=x_{3,0}/\lambda$, $p_{n,0,1}=f_1/mc$, $p_{n,0,3}=P_3(\xi=0)/(mc)$, etc. ($\lambda$ being the incoming wavelength). Also $\gamma_{n,1}=\gamma_1/mc=\gamma_0-p_{n,0,3}$, with $\gamma_0=[1-\boldsymbol{\beta}_0^2]^{-1/2}$ (the initial relativistic factor of the electron), and $s_n=s/c=[1+p_{n,0,1}^2+p_{n,0,2}^2]/2\gamma_{n,1}^2-1/2$. The index δ takes two values (L or C) corresponding to linear (L) or circular (C) polarization of the incoming light; $c_L=0$ and $c_C=1$. Then, $g_{n,\delta}$ ($n=0,1,2,3$) becomes

$$g_{0,\delta}=-\sin\theta_0\left[2\pi x_{n,0,1}+\frac{c_\delta\alpha}{2\pi\gamma_{n,1}}\right]+(1-\cos\theta_0)\times\left[2\pi x_{n,0,3}+\frac{\alpha(p_{n,0,1}c_\delta+p_{n,0,2}(1-c_\delta))}{2\pi\gamma_{n,1}^2}\right],$$

$$g_{1,\delta}=1-\sin\theta_0\left(\frac{p_{n,0,1}}{\gamma_{n,1}}\right)+\left(1-\cos\theta_0\right)\times\left[s_n+\frac{\alpha\left(p_{n,0,2}c_\delta+\dfrac{\alpha}{2\pi(2-c_\delta)^2}\right)}{2\pi\gamma_{n,1}^2}\right],$$

$$g_{2,\delta}\cos\varphi_\delta=-c_\delta(1-\cos\theta_0)\left(\frac{\alpha}{2\pi\gamma_{n,1}^2}\right)\left[p_{n,0,2}+\frac{\alpha}{2\pi}\right],$$

$$g_{2,\delta}\sin\varphi_\delta=\frac{\alpha}{2\pi}\frac{p_{n,0,2}}{\gamma_{n,1}^2}(1-c_\delta)(1-\cos\theta_0)+c_\delta\frac{\alpha}{2\pi}\left[-\frac{\sin\theta_0}{\gamma_{n,1}}+(1-\cos\theta_0)\frac{p_{n,0,1}}{\gamma_{n,1}^2}\right],$$

$$g_{3,\delta}=\frac{(1-c_\delta)(1-\cos\theta_0)}{2}\left(\frac{\alpha}{4\pi\gamma_{n,1}}\right)^2.$$

The coefficients appearing in Eqs. (28)–(41) are

$$q_{L,10}=p_{n,0,1},\quad q_{L,1n}=0,\quad n=\pm1,\pm2,$$

$$q_{L,20}=p_{n,0,2},\quad q_{L,2+1}=\frac{\alpha}{4\pi i}=-q_{L,2-1},\quad q_{L,2n}=0,\quad n=\pm2,$$

$$q_{L,30}=-\frac{\gamma_{n,1}}{2}+\frac{1+p_{n,0,1}^2+p_{n,0,2}^2}{2\gamma_{n,1}}+\frac{1}{\gamma_{n,1}}\left(\frac{\alpha}{4\pi}\right)^2,$$

$$q_{L,3+1}=\frac{\alpha}{4\pi i}\left(\frac{p_{n,0,2}}{\gamma_{n,1}}\right)=-q_{L,3-1},$$

$$q_{L,3+2}=-\frac{1}{2\gamma_{n,1}}\left(\frac{\alpha}{4\pi}\right)^2=q_{L,3-2},$$

$$q_{C,10}=p_{n,0,1},\quad q_{C,1+1}=\frac{\alpha}{4\pi i}=-q_{C,1-1},$$

$$q_{C,20}=p_{n,0,2}+\frac{\alpha}{2\pi},\quad q_{C,2+1}=-\frac{\alpha}{4\pi}=q_{C,2-1},$$

$$q_{C,30}=-\frac{\gamma_{n,1}}{2}+\frac{1+p_{n,0,1}^2+\left(p_{n,0,2}+\dfrac{\alpha}{2\pi}\right)^2}{2\gamma_{n,1}}+\frac{2}{\gamma_{n,1}}\left(\frac{\alpha}{4\pi}\right)^2,$$

$$q_{C,3+1}=\frac{\alpha}{4\pi\gamma_{n,1}}\left[\frac{p_{n,0,1}}{i}-\left(p_{n,0,2}+\frac{\alpha}{2\pi}\right)\right],$$

$$q_{C,3-1}=-\frac{\alpha}{4\pi\gamma_{n,1}}\left[\frac{p_{n,0,1}}{i}+\left(p_{n,0,2}+\frac{\alpha}{2\pi}\right)\right].$$

In terms of dimensionless variables, Eqs. (46) and (37) become

$$\frac{1}{F_C}=1-\frac{p_{n,0,1}\sin\theta_0}{\gamma_{n,1}}+(1-\cos\theta_0)\left[-\frac{1}{2}+\frac{1}{2\gamma_{n,1}^2}+\frac{p_{n,0,1}^2+(p_{n,0,2}+(\alpha/2\pi))^2+(\alpha/2\pi)^2}{2\gamma_{n,1}^2}\right],\tag{B1}$$

$$\frac{1}{F_L}=1-\frac{p_{n,0,1}\sin\theta_0}{\gamma_{n,1}}+(1-\cos\theta_0)\times\left[-\frac{1}{2}+\frac{1}{2\gamma_{n,1}^2}+\frac{p_{n,0,1}^2+p_{n,0,2}^2+2^{-1}(\alpha/2\pi)^2}{2\gamma_{n,1}^2}\right].\tag{B2}$$

APPENDIX C: $J_l(x,y)$ AND SOME PROPERTIES

Equation (26) (with $\theta-\varphi\to\theta$) coincides exactly with Eq. (2) in Ref. 25. By multiplying both sides of Eq. (26) by $\exp[-im\psi]$ ($\psi=\theta-\varphi$ and m being an integer), integrating over ψ in $-\pi\le\psi\le\pi$ and using $\int_{-\pi}^{+\pi}d\psi\exp[i(l-m)\psi]=2\pi\delta_{lm}$, δ_{lm} being the Kronecker delta, one finds

$$J_l(x,y)=\int_{-\pi}^{\pi}\frac{d\psi}{2\pi}\exp[i(x\sin\psi-y\sin2\psi-l\psi)].\tag{C1}$$

This representation for the generalised Bessel Functions has the advantage of explicity showing that $J_l(x,y)$ is a real function. In fact, the imaginary part in Eq. (C1) vanishes, since it is an odd function integrated over a symmetric interval. Equation (26) can also be used to obtain an expression for the generalised Bessel function $J_l(x,y)$ in terms of ordinary Bessel functions. In fact, we start from Eq. (26) (with $\varphi=0$), expand both factors in its left-hand-side by using Eq. (39), multiply by $\exp[-il\theta]$ (l being an integer), and integrate over θ in $-\pi\le\theta\le\pi$. The desired result reads

$$J_l(x,y)=\sum_{m=-\infty}^{+\infty}(-1)^mJ_{l-2m}(x)J_m(y).\tag{C2}$$

One readily gets $J_{-l}(x,y)=J_l(-x,-y)$ and $J_l(-x,y)=(-)^lJ_l(x,y)$. Formula (C1) could serve as a basis for very efficient computation of those functions, in particular if their arguments (x and y) are not very large. In that case, a power series expansion of the term $\exp[i(x\sin\psi-y\sin2\psi-l\psi)]$ under the integral allows for an efficient computation of Eq. (C1) up to the desired level of precision. It can be easily seen that $J_l(x,y)$ reduces to the ordinary Bessel function $J_l(x)$ for $y=0$.

[1]D. H. Froula, S. H. Glenzer, N. C. Luhmann, Jr., and J. Sheffield, *Plasma Scattering of Electromagnetic Radiation: Theory and Measurement Techniques* (Academic, Elsevier, Amsterdam, 2011).

[2]I. Hutchison, *Principles of Plasma Diagnostics* (Cambridge University Press, Cambridge, 2005).
[3]D. E. Evans and J. Katzenstein, Rep. Prog. Phys. **32**, 207 (1969).
[4]M. Mattioli, "Incoherent Light Scattering from High Temperature Plasmas," Report DPh-PFC-SPP, (EUR-CEA-FC) 752, 1974.
[5]T. Matoba, T. Itagaki, T. Yamauchi, and A. Funahashi, Jpn. J. Appl. Phys., Part 118, 1127 (1979).
[6]B. Weyssow, J. Plasma Phys. **43**, 119 (1990).
[7]O. Naito, H. Yoshida, and T. Matoba, Phys. Fluids B **5**, 4256 (1993).
[8]K. V. Beausang and S. L. Prunty, Plasma Phys. Controlled Fusion **50**, 095001 (2008).
[9]M. J. Walsh, Rev. Sci. Instrum. **77**, 10E525 (2006).
[10]J. S. Ross, S. H. Glenzer, J. P. Palastro, B. B. Pollock, D. Price, L. Divol, G. R. Tynan, and D. H. Froula, Phys. Rev. Lett. **104**, 105001 (2010).
[11]J. P. Palastro, J. S. Ross, B. Pollock, L. Divol, D. H. Froula, and S. H. Glenzer, Phys. Rev. E **81**, 036411 (2010).
[12]L. D. Landau and E. M. Lifchitz, *The Classical Theory of Fields*, 4th ed. (Pergamon, New York, 1975).
[13]E. S. Sarachik and G. T. Schappert, Phys. Rev. D **1**, 2738 (1970).
[14]E. Essarey, S. K. Ride, and P. Sprangle, Phys. Rev. E **48**, 3003 (1993).
[15]S. K. Ride, E. Essarey, and M. Baine, Phys. Rev. E **52**, 5425 (1995).
[16]C. A. Brau, *Modern Problems in Classical Electrodynamics* (Oxford University Press, Oxford, 2004).
[17]H. K. Avetissian, *Relativistic Nonlinear Electrodynamics, Springer Series in Optical Sciences* (Springer, New York, 2006).
[18]J.-H. Yang, R. S. Craxton, and M. G. Haines, Plasma Phys. Controlled Fusion **53**, 125006 (2011).
[19]W. K. H. Panofsky and M. Phillips, *Classical Electricity and Magnetism* (Addison-Wesley, Reading, MA, 1955).
[20]I. Pastor, J. Guasp, R. F. Alvarez-Estrada, and F. Castejon, Nucl. Fusion **51**, 043011 (2011).
[21]J. D. Jackson, *Classical Electrodynamics*, 2nd ed. (Wiley, New York, 1974).
[22]R. F. Alvarez-Estrada and E. R. Martinez, An. Fis. **77**, 110 (1981).
[23]P. J. Duke, *Synchrotron Radiation: Production and Properties*, Oxford Science Publications (Oxford University Press, Oxford, 2000).
[24]F. W. J. Olver, "Bessel functions of integer order," in *Handbook of Mathematical Functions*, edited by M. Abramowitz and I. A. Stegun (Dover, New York, 1965).
[25]E. Loetstedt and U. D. Jentschura, Phys. Rev. E **79**, 026707 (2009).